Functional Imaging of the Lungs With Gas Agents

Stanley J. Kruger, PhD,[1] Scott K. Nagle, MD, PhD,[1,2,3] Marcus J. Couch, MSc,[4,5] Yoshiharu Ohno, MD, PhD,[6] Mitchell Albert, PhD,[4,7] and Sean B. Fain, PhD[1,2,8]*

This review focuses on the state-of-the-art of the three major classes of gas contrast agents used in magnetic resonance imaging (MRI)—hyperpolarized (HP) gas, molecular oxygen, and fluorinated gas—and their application to clinical pulmonary research. During the past several years there has been accelerated development of pulmonary MRI. This has been driven in part by concerns regarding ionizing radiation using multidetector computed tomography (CT). However, MRI also offers capabilities for fast multispectral and functional imaging using gas agents that are not technically feasible with CT. Recent improvements in gradient performance and radial acquisition methods using ultrashort echo time (UTE) have contributed to advances in these functional pulmonary MRI techniques. The relative strengths and weaknesses of the main functional imaging methods and gas agents are compared and applications to measures of ventilation, diffusion, and gas exchange are presented. Functional lung MRI methods using these gas agents are improving our understanding of a wide range of chronic lung diseases, including chronic obstructive pulmonary disease, asthma, and cystic fibrosis in both adults and children.

J. MAGN. RESON. IMAGING 2016;43:295–315.

Pulmonary magnetic resonance imaging (MRI) has conventionally been limited by a low signal-to-noise ratio (SNR) in the lung parenchyma. This limitation stems from the combined effects of low proton density and high local susceptibility induced by the numerous air–tissue interfaces intrinsic to the lung parenchyma that facilitate gas exchange. For conventional proton MRI, the former limits the available number of spins per unit volume while the latter creates local field inhomogeneity that contributes to very short T_2^* decay times on the order of 1–2 msec.[1] In part because of these challenges, significant research focus has been dedicated to developing methods to enhance contrast in the lungs, particularly in the lung parenchyma. Oxygen-enhanced (OE) and fluorinated gas MRI were introduced in the early 1990s[2,3] for imaging lung function, principally ventilation-weighted imaging, but were not widely disseminated. Hyperpolarized (HP) gas MRI, particularly ^{3}He and more recently ^{129}Xe, gases are comparatively more mature, having been demonstrated to provide a wider array of functional contrasts inclusive of spin density, diffusion-weighted imaging, and gas exchange, each with demonstrated applications to different obstructive and restrictive lung diseases in clinical research,[4,5] and yet despite these established roles for HP gas imaging, clinical dissemination and impact in the clinic has been limited.

More recently, the outlook for pulmonary MRI is improving due largely to the increased performance of gradient systems and constrained reconstruction methods[6–9] that have enabled 3D high spatial resolution (~1 mm) MRI of lung structures with improved contrast and coverage.[10–12] The recently developed preclinical[13,14] and clinical[15–17] ultrashort echo time (UTE) methods and short repetition time (TR) methods[18,19] are largely robust to motion and demonstrate improved lung signal for both structural and functional lung MRI (FLI) applications by mitigating the effects of T_2^* decay. For HP gases, there has been a resolution in the commercial uncertainty on the availability of polarizer systems[5] improving the outlook for wider dissemination of HP ^{129}Xe technologies.

View this article online at wileyonlinelibrary.com. DOI: 10.1002/jmri.25002

Received Feb 2, 2015, Accepted for publication Jun 26, 2015.

*Address reprint requests to: S.B.F., 1111 Highland Ave., Rm. 1005, Madison, WI 53705-2275. E-mail sfain@wisc.edu

From the [1]Department of Medical Physics, University of Wisconsin, Madison, Wisconsin, USA; [2]Department of Radiology, University of Wisconsin, Madison, Wisconsin, USA; [3]Department of Pediatrics, University of Wisconsin, Madison, Wisconsin, USA; [4]Thunder Bay Regional Research Institute, Thunder Bay, Ontario, Canada; [5]Biotechnology Program, Lakehead University, Thunder Bay, Ontario, Canada; [6]Department of Radiology, Kobe University Graduate School of Medicine, Kobe, Japan; [7]Department of Chemistry, Lakehead University, Thunder Bay, Ontario, Canada; and [8]Department of Biomedical Engineering, University of Wisconsin, Madison, Wisconsin, USA

The structure of this review focuses on technical tradeoffs and principal applications of the most common FLI methods using HP gas, fluorinated gas, and OE MRI. First, a rationale for FLI is discussed in the context of current clinical measures of whole lung function. Second, the physical properties of the gas agents are discussed and how these properties influence imaging strategy and types of imaging contrast. Third, specific tradeoffs in terms of cost, availability, and capability are discussed. The final sections review the major clinical research applications explored thus far using each of HP, fluorinated, and OE methods, respectively.

Lung Function and Imaging

An important potential role for FLI is to provide regional information regarding diseases affecting ventilation and gas exchange. Inexpensive whole-lung spirometry and plethesmography measures, commonly referred to as "pulmonary function tests" or PFTs, are derived from respiratory maneuvers designed to measure fixed lung volumes and dynamic airflow curves. However, PFTs have well-known limitations in that they measure average obstruction over the whole lung and reveal only limited information about regional distribution or spatial heterogeneity of obstructive disease. Most common among spirometry measures are forced expiratory volume at 1 second (FEV_1) and FEV_1 normalized to forced vital capacity (FEV_1/FVC).[20] Both FEV_1 and FEV_1/FVC are reduced in obstructive disease because the large and small airways in the lungs have increased resistance to air flow, limiting both the total volume of air exhaled and the rate of exhaled air flow.[20] Plethesmography, using Boyle's Law and a "body box",[20] is used to measure absolute lung volumes include the total lung capacity (TLC), functional residual capacity (FRC), and residual volume (RV) that are typically increased in obstructive disease due to hyperventilation and air trapping, respectively.[21] However, PFTs are standardized with commonly agreed-upon reference values for different populations, gender, and body size.[22,23] This standardization to normative values is an important strength that makes it possible to make general comparisons of disease severity across different populations—this and the low cost of conventional PFTs make them attractive as a means to screen for and monitor disease progression.

Several more refined measures of whole lung function are important but less commonly used. These include the carbon monoxide diffusing capacity (DLCO) method that exploits the high chemical affinity of carbon monoxide (CO) for blood hemoglobin. Specifically, DLCO measures the difference between trace amounts of a known inhaled and exhaled concentration of CO. DLCO is affected by reduced alveolar surface area to volume ratio (eg, emphysema) or by diffusion-block (eg, fibrotic lung disease)[24] and therefore can be a useful measure for quantifying lung function and severity of chronic lung diseases such as chronic obstructive pulmonary disease (COPD) and idiopathic pulmonary fibrosis (IPF). Lung clearance index (LCI) is another whole-lung measure that is an emerging standard for improving quantitative assessment of ventilation heterogeneity in obstructive lung diseases such as asthma and the pulmonary complications of cystic fibrosis (CF).[25] The method uses the multiple breath nitrogen washout method[20] and is considered sensitive to ventilation heterogeneity because the delay in oxygen wash-in reaching nonventilated units of the lungs prolongs the nitrogen washout time (normally ~7 minutes).

However, the insensitivity of these conventional PFTs to early disease has driven pulmonary clinicians and radiologists to seek measures that are more sensitive to regional and early disease processes. The role for FLI using MRI has therefore continued to grow, especially in clinical research of regional disease processes in asthma, CF, and COPD with an eye towards improving treatments. According to the World Health Organization, over 65 million people have moderate to severe COPD worldwide. More than 3 million people died of COPD in 2005, which corresponds to 5% of all deaths globally (http://www.who.int/respiratory/copd/burden/en/). Over 235 million people suffer from asthma, and asthma is the most common chronic disease among children (http://www.who.int/respiratory/asthma/en/). CF, while a comparatively rare obstructive lung disease, is also an important pediatric lung disease. There is a prominent role for MRI to reduce ionizing radiation during surveillance and to guide more precise drug therapy in CF especially (http://www.cff.org/research/DrugDevelopmentPipeline). In all three major obstructive lung diseases, there is a growing clinical need to improve the precision of therapies tailored to specific airways,[26,27] lung regions,[28] and/or phenotypes of lung disease.

Multiple methods of FLI using MRI exist, with tradeoffs and imaging strategies that are dependent on the properties of the gas used. The most mature of these are the HP gases, ^{3}He and ^{129}Xe, but the new implementations of OE and fluorinated gas methods are reemerging as competitive alternatives thanks to technical advances in scanner hardware and software that enable dynamic imaging of gas wash-in and washout. These advances have further improved the traditional advantages of MRI over nuclear medicine such as higher 3D spatial and temporal resolution and nonionizing radiation.[29] Improved 3D temporal-spatial resolution of pulmonary UTE MRI is now approaching that of computed tomography (CT),[15] while the myriad of tools for assessing lung function exceed those available with CT.[30] These factors coupled with concerns over x-ray radiation dose for longitudinal studies using CT have made MRI especially attractive for pediatric and young adult populations.[31–33]

Gas Properties and Imaging Strategies

The physical properties of the gases, their natural abundance, and method of manufacture require different imaging

TABLE 1. Physical Parameters for the Most Common Gas Contrast Agents Used for Pulmonary MRI

	HP ^{3}He	HP ^{129}Xe	$^{1}H/O_2$ Enhanced	SF_6	C_2F_6
Nuclear gyromagnetic ratio (MHz/T)	33.434	11.777	42.576[a]	40.052	40.052
Polarization	30-40%	8-25%	~1 ppm[d]	~1 ppm[d]	~1 ppm[d]
Diffusion coefficient – free (cm^2/s)	2.05[154]	0.062[154]	0.176[234]	0.033[214]	0.033[216]
Apparent diffusion coefficient – ADC (cm^2/s)	0.16[154]	0.021[154]	[b]	0.0222c[69]	0.018c[216]
Density of the gas (g/cm^3)	1.34×10^{-4}	5.75×10^{-3}	1.43×10^{-3}	6.51×10^{-3}	6.16×10^{-3}
Normoxic or anoxic dose	Anoxic	Anoxic	Norm/hyperoxic	Normoxic	Normoxic
Volume required for typical study	1 L	1 L	300 L	5 L	5 L
Partition coefficient in blood (Ostwald – unitless)	0.0085[235]	0.17[235]	0.0261[235]	0.0075[235]	0.001273[236]

HP: hyperpolarized; SF_6: sulfur hexafluoride gas; C_2F_6: hexafluoroethane gas; ppm – part per million nuclei.
[a]Via paramagnetic effect on proton signal.
[b]No value in the literature.
[c]Derived from pre-clinical rat studies.
[d]Field strength-dependent - value is approximate for $B_0 = 1.5$ T.

strategies and cost models. The SNR and spatial resolution are governed largely by physical parameters such as the degree of polarization, gyromagnetic ratio, free diffusion coefficient, T_1, and T_2 (Tables 1, 2). For HP ^{3}He and ^{129}Xe, the nonrecoverable longitudinal polarization of the gas nuclei is ~100,000 times greater than thermal equilibrium. This HP state is achieved typically using the spin exchange optical pumping (SEOP) method.[34–36] The effective T_1 time for imaging in the lungs is ~30 seconds (Table 2), allowing sufficient time for acquisition within a breath-hold.

Inert ^{19}F gases, on the other hand, are not hyperpolarized but are still used for ventilation imaging. Fluorinated gases are an attractive choice because the ^{19}F isotope is 100% naturally abundant, with a high gyromagnetic ratio (Table 1) on the order of that of ^{1}H[37] The T_1 relaxation is dominated by spin-rotation interactions,[38] $T_1 \sim T_2$ (Table 2). Both magnetic resonance decay parameters depend on the concentration of the gas itself and are generally on the order of a few milliseconds for the ^{19}F nucleus. The most commonly used fluorinated gases are sulfur hexafluoride (SF_6) and hexafluoroethane (C_2F_6), but tetrafluoromethane (CF_4) and octafluoropropane (C_3F_8) are also under investigation. T_1 and T_2 values at or near the 1.5T field strength are less than 6 msec for C_2F_6, and as low as 2 msec for SF_6. C_3F_8 is of particular interest because it possesses two additional fluorine atoms, providing greater spin density[39] and similarly short T_1 and T_2.[38]

TABLE 2. MRI Longitudinal and Transverse Decay Constants in the Lungs and at the Field Strength Indicated for the Most Common Gas Contrast Agents

	Value						
	HP ^{3}He	HP ^{129}Xe	Normoxic ^{1}H (21%)	Hyperoxic ^{1}H (100%)	SF_6	C_2F_6	C_3F_8
Field Strength (T)	1.5	1.5	1.5	1.5	1.5	1.9	1.5
T1 (msec)	32,000[237]	20,000[214]	1,237[77]	1,129[77]	1.2[214]	5.9[3]	18[38]
T2 (msec)	2,000[238]	310[239]	30[240]	[a]	[a]	5.9	16[38]
T2* (msec)	20[241]	18.5[63]	1.8[75]	1.6[75]	1.0[209]	[a]	[a]

HP: hyperpolarized; SF_6: sulfur hexafluoride gas; C_2F_6: hexafluoroethane gas.
[a]No value in the literature.

Both HP and fluorinated gases are imaged directly and their T_1 properties lend themselves to fast imaging with low flip angle gradient-recalled-echo (GRE), also known as fast-low-angle-shot (FLASH), pulse sequences for 2D multi-slice[40,41] or 3D volumetric[42,43] imaging with Cartesian or radial acquisition trajectories.[44] For HP gases, the nonrecoverable longitudinal polarization can be excited frequently with low flip angle acquisitions, with the consequence that signal decay due to the radiofrequency (RF) consumption of the magnetization is known to contribute to signal modulation and filtering of both slice profile and within-slice blurring.[41] RF signal modulation due to a constant flip angle can be offset by precise flip angle modulation[45,46] but is infrequently used in favor of simply using low flip angles (~2–7°) and centric view ordering.[47,48] For fluorinated gases, T_1 is short enough (~1–20 msec, Table 1) that fast GRE or FLASH sequences are also signal-to-noise and time efficient.[49–52] For dynamic imaging applications using both HP and fluorinated gases, fast low flip angle GRE sequences with non-Cartesian readout trajectories that frequently sample the central region of *k*-space are used. Time-resolved 2D radial,[44] spiral,[53] or 3D radial spoiled GRE sequences with isotropic resolution[49,54] and constrained reconstruction[54–56] have been used.

The comparatively longer T_2 of HP gases vs. the short T_1 and T_2 of fluorinated gases make them favorable for SNR-efficient balanced steady-state free precession (SSFP) imaging, although optimizing flip angle and T_2 raise additional challenges.[46] Recent advances combining SSFP imaging with cheaper natural abundance (~26%) HP ^{129}Xe gas has recently shown promise for ventilation-weighted imaging.[57] Parallel imaging with HP gases has also been explored[58–61] but widespread implementation has been slowed by hardware costs for multichannel RF-coils and compatibility with multinuclear clinical MRI systems. This is a ripe area for future advances in FLI using both HP and fluorinated gases.

Diffusion-weighted imaging (DWI) has been one of the most promising FLI tools to investigate lung microstructure in normal and diseased lungs. The physical diffusion coefficients differ markedly for HP ^{3}He, ^{129}Xe, and for fluorinated gases (Table 1), which strongly impacts utility. The greater free diffusion coefficients and polarization of HP ^{3}He and ^{129}Xe gases enable rapid measurement of multiple b-values using existing clinical gradient systems[62,63] using fast GRE pulse sequences with bipolar diffusion weighting gradients. The separation, Δ, between these short bipolar gradient pulses determines the diffusion weighting as well as the dependence of the diffusion measures on the scale of restricted diffusion displacement. For helium the average displacement of helium atoms using $\Delta = 1$–2 msec is the same order of magnitude as alveolar diameters (a few hundred micrometers). This so-called "short range ADC" measure is the one most widely used in patient studies.[64] Additional b-value weightings can be acquired using HP ^{3}He to enable more precise modeling of restricted diffusion either using q-space[55,65] or model-based techniques.[66]

DWI for denser HP ^{129}Xe[5] and fluorinated gases[67–69] is possible, but their lower free diffusivity and short T_2^* make high gradient performance to increase b-value, reduce TE, and preserve sufficient SNR particularly important making multi-b-value DWI challenging. Advances in radial free induction decay (FID) acquisitions may help meet these challenges and are typically used in DWI of fluorinated gases, as the short TE and TR help to exploit the short T_1 recovery times while mitigating T_2* decay.

Another important physical distinction is gas solubility in tissues and blood. Both HP ^{129}Xe and molecular O_2 are relatively soluble in blood and tissues compared to HP ^{3}He and fluorinated gases (Table 1). Therefore, ^{129}Xe and O_2 diffuse from the gas phase into the tissues and blood where they reflect useful properties of the local spin environment. Image contrast for both of these gases represents a combination of ventilation, tissue density, blood volume, and perfusion. In the specific case of HP ^{129}Xe, the 200 ppm chemical shift associated with the dissolved phase (Fig. 1) can be imaged directly[10,70,71] or indirectly[72,73] to enable quantitative modeling of gas exchange.

Unlike HP ^{129}Xe, the OE effect is based on the concentration-dependent paramagnetic effect of dissolved molecular oxygen on the rate of T_1 recovery of protons.[2,74] Note that this is not the diamagnetic effect of hemoglobin-bound oxygen that results in the T_2*-effect commonly associated with blood oxygenation level-dependent (BOLD) MRI.[75,76] FLASH or GRE sequences can be used to perform rapid T_1 mapping at multiple O_2 concentrations to derive the oxygen transfer function (OTF) measure.[77–79] More typically, OE-MRI methods have favored inversion-recovery (IR) pulse sequences in combination with single-shot fast spin-echo (SSFSE), to exploit the ~30 msec T_2 of protons in the lungs (Table 2) compared to the much lower T_2*. For IR-SSFSE in this application, the TI is typically set to the null point of the lungs in the air-breathing image[2,80,81] or to maximize the contrast between the T_1 recovery curves.[82–86] Centric view ordering reduces the effects of T_2 decay and provides better contrast in the OE image. Using this approach, the image of a single 2D slice can be acquired in a fraction of a second, but the low contrast of OE MRI requires signal averaging on the order of 10+ minutes for a complete OE scan. Prospective respiratory gating to end-expiration and retrospective deformable image registration combined with interleaved 2D slices, parallel imaging, and half-Fourier reconstruction have enabled multislice 2D OE-MRI using IR-SSFSE in 8–13-minute total scan times.[85]

The emergence of UTE MRI with clinical hardware systems has advanced both structural and functional imaging of the lungs with varied impact thus far on FLI using all

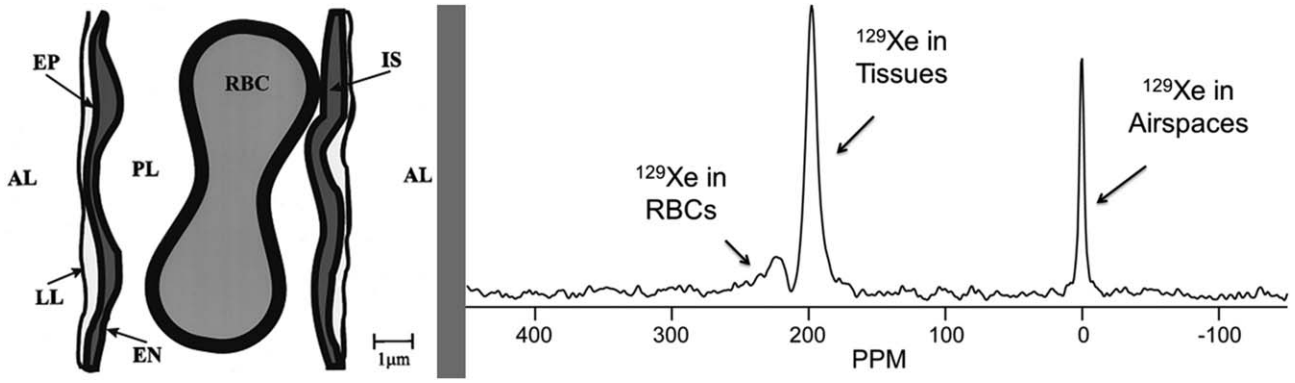

FIGURE 1: (a) Schematic of the tissue-capillary boundary. Gas phase is contained within the alveoli (AL). Septal wall comprises the liquid lining (LL), tissue epithelium (EP), interstitial space (IS), and tissue endothelium (EN). Blood volume comprises the PL = blood plasma, and RBC = red blood cells (adapted from [72]). (b) ^{129}Xe MR spectrum from the human lung with peaks corresponding to the gas, plasma-tissue, and red blood cell (RBC) compartments. Note that the spectral peak for the ^{129}Xe gas in the airspaces is attenuated by a factor of ~100 by using a lower flip angle relative to the dissolved phases.

three gas agents. For OE-MRI, T_1 weighting can now be achieved without IR using 3D radial UTE.[11,14,15] Radial acquisitions in FLI more generally are inherently robust against cardiac motion artifact due to the large number of signal averages at the center of *k*-space per unit time. UTE combined with radial trajectories has recently contributed to important advances in fluorinated gas MRI by improving image quality, coverage, and reducing scan time,[3,87,88] and to HP gas MRI for spectroscopic imaging of the dissolved phases of HP ^{129}Xe in the tissue and blood compartments.[10,70,71]

Tradeoffs in Cost and Access

A well-known disadvantage of HP ^{129}Xe and ^{3}He is their dependence on polarizer and multinuclear technology that is not widely available.[4] The global quantities of ^{3}He are also very limited, leading to high cost[89] (Table 3). This fact has necessitated migration to the more widely available ^{129}Xe nucleus.[90] The technical challenges of this migration have been made easier by advances in ^{129}Xe SEOP polarization.[91,92] Most typically, HP ^{129}Xe MRI uses enriched ^{129}Xe isotope from the natural abundance of 26% to ~85% to compensate for lower gyromagnetic ratio and achievable polarization compared to ^{3}He gas. All the major types of contrast-weighting demonstrated for ^{3}He MRI have now been replicated robustly with enriched HP ^{129}Xe.[5,93]

High SNR, the availability of different functional contrasts, and ease of use in terms of gas delivery and image acquisition are important advantages of HP gas MRI (Table 3). The HP gases are most commonly delivered as an anoxic gas mixture to the subject followed by a 6–15-second breath-hold, although it is possible to mix with O_2 at the mouth to make a normoxic dose.[94] The repeatability and utility of quantitative measures of ventilation defect percentage (VDP) is high (Fig. 2), but depend on normalization of the ventilation-weighted images by the total lung volume (TLV) typically acquired from a proton image of the lungs during a second breath-hold. Misregistration can occur between breath-holds, adding systematic error to the ventilation defect measurement. Recently, acquiring both HP gas and proton images of the TLV in spatial registration within the same breath-hold was demonstrated.[95] Extensive experience with HP ^{3}He MRI and now ^{129}Xe has shown that repeated inhalation of these gases is safe.[93,96–98] The anesthetic effects of xenon are not a concern in adult subjects[98] but remain to be studied in pediatric lung disease. Since ^{3}He gas has been safely used in a wide range of pediatric studies,[99–101] it will likely remain an important gas during the translation of ^{129}Xe to pediatric lung disease.[100] Additionally, improved polarization methods for ^{129}Xe[92,102] may eventually make the use of natural abundance HP ^{129}Xe MRI feasible,[57] significantly reducing cost (Table 3). There are now two companies developing commercial HP ^{129}Xe polarizers and technology for lung imaging applications: Xemed LLC (http://www.xemed.com/) and Polarean (http://www.polarean.com/). In addition, an open source ^{129}Xe polarizer system that can be manufactured locally using 3D printing technology was introduced recently.[102,103]

Despite the advantages and more positive outlook for HP ^{129}Xe gas, fluorinated and oxygen gases are inexpensive by comparison. Oxygen is already widely available in the clinical environment, including most MRI suites, requiring no specialized hardware modifications to clinical scanners. Both low cost and accessibility support the high potential of OE-MRI for widespread dissemination (Table 3). Fluorinated gases fall somewhere between HP gases and oxygen on the scale of cost and technical complexity. The gases themselves are relatively inexpensive, but dedicated multinuclear transmit and receive RF coils are required. Fluorinated gases compare favorably to HP gases in that scan times can be relatively short (12–15 sec), but the method requires respiratory-controlled breathing to enable multiple breath wash-in to reach a normoxic steady-state breath-hold with sufficient SNR.[104]

OE-MRI would likely be the clear winner if limitations of lower SNR could be robustly overcome within a

TABLE 3. Strengths and Challenges of Different Gas Contrast Agents for Pulmonary Functional Imaging

	HP He-3 MRI	HP Xe-129 MRI	OE MRI	F-19 MRI
SNR	High	Med-High	Low	Low
Breath-hold imaging	Yes	Yes	No	Yes*
Cost	~$800-1200/L	$170/L (enriched) $15/L (natural abundance)	<$1/L	$15-20/L
Hardware requirements	MNS T/R Polarizer	MNS T/R Polarizer	Conventional Clinical MRI	MNS T/R
IND required	Yes	Yes	No	Yes
Scan length	5-10 s	5-10 s	5-30 min	12-15 s
Typical spatial resolution	3 mm×3 mm×10 mm	3 mm×3 mm×10 mm	2 mm×2 mm×10 mm	6 mm×6 mm×15 mm
Most common quantitative measures	ADC, VDP, pO_2	ADC, VDP, pO2	MRSER, PSE, OTF	VDP
Repeatability established	Yes	Yes	No	No
Signal weightings	Ventilation, diffusion, oxygen mapping	Ventilation, diffusion, oxygen mapping, Gas exchange	Ventilation and perfusion	Ventilation and Oxygen mapping
Clinical research strengths	High spatial-temporal resolution regional measures of emphysema and gas trapping and airflow obstruction.	Regional measures of emphysema and gas trapping and airflow obstruction. Dissolved phases in tissue and blood are a measure of gas exchange.	Inexpensive, widely accessible method for ventilation weighted imaging. Potential for quantitative ventilation.	Less expensive method for ventilation weighted imaging. Potential for quantitative ventilation.

HP: hyperpolarized; OE: oxygen-enhanced; SNR: signal to noise ratio; IND: Investigational New Drug (FDA) application; ADC: apparent diffusion coefficient; VDP: ventilation defect percentage; pO2: oxygen partial pressure; MRSER: mean relative signal enhancement ratio; PSE: percent signal enhancement; OTF: oxygen transfer function; V/Q: ventilation-to-perfusion ratio. *After multiple breath-wash-in to approach steady-state.

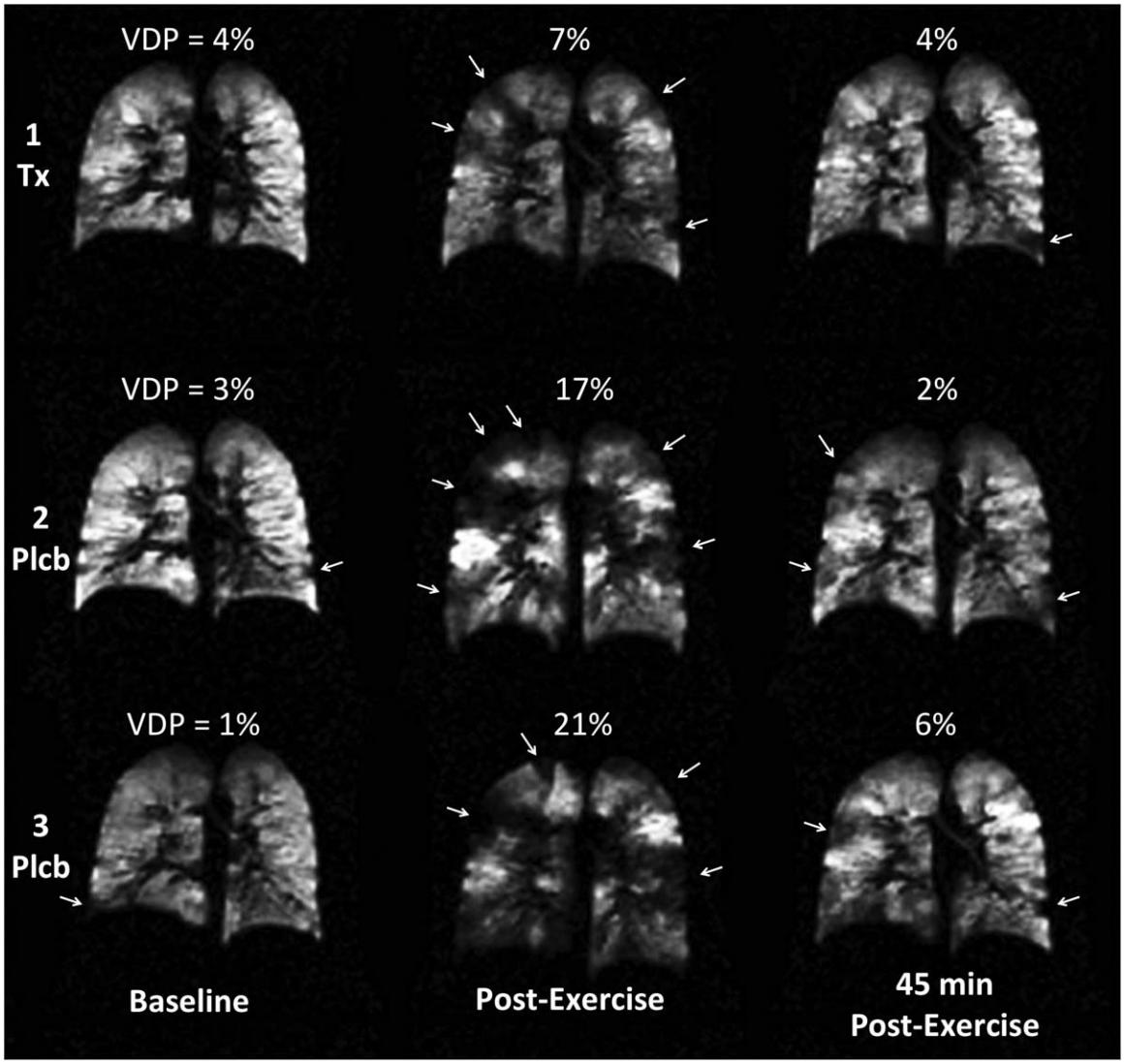

FIGURE 2: ^{3}He MRI lung images showing a strong VDP response to challenge pre- (baseline) and postexercise challenge in a subject with exercise-induced bronchoconstriction and treatment with Montelukast (visit 1 vs. visits 2 and 3). Defects (arrows) occur most prominently after exercise challenge and postchallenge decreases in FEV_1 for this subject coincide with increases in VDP as indicated. Recovery 45 minutes postexercise shows residual VDP for visit 3. Overall, residual VDP after recovery was significantly higher on ^{3}He MRI compared to baseline but FEV_1 recovered back to baseline. Plcb = placebo visit; Tx = treatment visit. Adapted from Ref. 144 with permission.

clinically feasible workflow. However, the advantages of cost and accessibility are offset by the more complex gas delivery and longer acquisition time. Proton spins in the vicinity of dissolved oxygen have a modest T_1 difference of 8–15%,[2,77,82,86] and as for fluorinated gases, the OE effect is not instantaneous, requiring a physiological wash-in and washout with time constant ranging from as long as 45–50 seconds[79,105] to as low as 17–30 seconds.[74,106,107] It is therefore necessary to signal average over multiple breaths. Respiratory and cardiac motion must be addressed either prospectively or retrospectively. Usually, a dual acquisition is performed: one during inhalation of 21% O_2 (normal atmospheric oxygen concentration) and the other during inhalation of 100% O_2 (Fig. 3). Most researchers allow 1–2 minutes between changes in fractions of inhaled O_2 to avoid transient effects. Well-ventilated regions of the lung show an oxygen-dependent signal enhancement; typically, a map of this signal enhancement is provided in units of percent signal enhancement. Both respiratory[108] and cardiac triggering have been implemented successfully for 2D OE-MRI.[85,109] Typically, nonrebreather facemasks are used with a constant flow of oxygen at 15 L/min.[110,111] Even with the use of respiratory gating or triggering, lung volume can vary with changes in the fraction of inhaled O_2.[112] Since most complete OE-MRI datasets take 10 or more minutes to acquire, this fact combined with bulk patient motion can cause misregistration between the two sets of images. Initially, many researchers performed signal averaging by taking advantage of the large number of acquired images to blur the misregistration, particularly near the diaphragm.[77,80,113] Since then, Mai et al[84] demonstrated an improved correlation between the fraction of inhaled O_2 input function and the OE-MRI signal by using only the images with minimal divergence in diaphragm position. The majority of

researchers have implemented this approach prior to signal averaging—in effect implementing a combination of both prospective and retrospective respiratory gating.[2,82,106,109,114,115] More recently, diffeomorphic registration[116,117] has been applied to 3D isotropic OE MRI.[11]

Applications

Hyperpolarized Gases

The MR physics of imaging with polarized gases have been extensively treated elsewhere,[5,34–36,41,92,100,118–126] so we here focus on contrast mechanisms and their applications in clinical research.

IMAGES OF VENTILATION. Spin density images during breath-hold represent a snapshot of gas distribution. The resulting "ventilation defects" (Fig. 2) are influenced by regional airway obstruction and air trapping.[127,128] The ventilation defect volume,[127,129,130] ventilated volume,[129,131] and coefficient of variation[132,133] derived from these images have all proven useful for demonstrating regional heterogeneity of ventilation in a wide range of obstructive lung diseases. Measures of ventilation defects are also sensitive to subclinical decline in function due to aging in healthy never-smokers[128,133] as well as smokers.[134–136] One semiautomated measure that is emerging as a biomarker is the VDP, defined as the defected lung volume normalized by the TLV.[137–140] Multiple groups have demonstrated the repeatability[130,139,141,142] and validity of this measure compared to pulmonary function testing[130,133,143–145] and severity of disease.[133,143,145] It should be noted that larger values for VDP are observed with ^{129}Xe MRI than with ^{3}He MRI in the same individual.[146] This bias is likely attributable to the difference in gas densities (Table 1), although this remains a matter for speculation and further research.[147]

DIFFUSION-WEIGHTED IMAGING (DWI). DWI exploits the high free diffusion of ^{3}He and ^{129}Xe gases. In the context of restriction by the lung microstructure, this allows indirect measurement of the average dimensions of the lung airspaces. When ^{3}He or ^{129}Xe gas is restricted by tissue boundaries, the diffusivity is referred to as the apparent diffusion coefficient (ADC). A semiquantitative ADC map (Fig. 4)—a surrogate for airspace size—is easily derived. Regional ADC changes have been observed in response to increases in lung volume,[148,149] gravity dependence,[148,150,151] age,[152] and etiology of emphysema, ie, COPD or alph1-antitrypsin.[122,131,150,153] Values for ^{3}He ADC in the lungs range from 0.66 cm^2/s for an elderly COPD patient (FEV_1 26% predicted) to as low as 0.16 cm^2/s for a young nonsmoker. For reference, the free diffusion coefficient of pure ^{3}He is 2.05 cm^2/s and ~0.8 cm^2/s in air mixture.[154] Values for ^{129}Xe ADC, by comparison, are lower than ^{3}He ADC by an order of magnitude, due to the higher density of ^{129}Xe gas (Table 1). For example, the ^{129}Xe ADC is 0.021 cm^2/s for a young nonsmoker, compared with 0.16 cm^2/s for ^{3}He ADC.

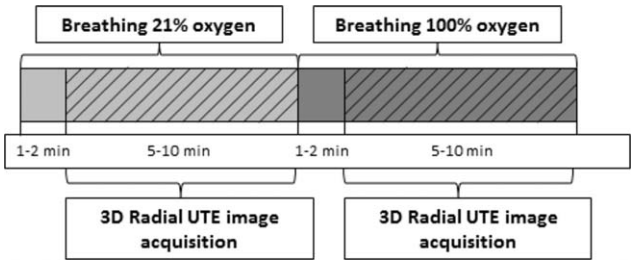

FIGURE 3: Timing and general protocol for oxygen-enhanced MRI as performed in Kruger et al.[11] Typically, images are acquired at different concentrations of inhaled oxygen (usually 21% and 100%), with a 1–2 minute washout period to avoid transient effects. Similar approaches are used for other OE-MRI acquisition techniques.

Despite the differences in the magnitude of the measured ADC using ^{3}He and ^{129}Xe, the ^{129}Xe ADC in human subjects is strongly associated with increased COPD severity and correlates well with ^{3}He ADC reported in previous studies.[93,147,151]

An important limitation of ADC is that it represents a *relative* measure of structural dimension that is *proportional* to the average alveolar and acinar dimensions. Its absolute value depends on specific scan parameters, such as the time delay and degree of diffusion weighting. A more quantitative measure of acinar dimensions would be very useful in answering several important physiologic questions regarding lung development,[65,99] alveolarization,[155] and alveolar recruitment.[156] Lung models of restricted diffusion that allow calculation of measurable histological features such as alveolar mean length and surface area to volume are in development[55,65,157–159] and have been reviewed previously.[66] More refined models that account for terminal airway branching[159,160] have stimulated healthy debate[161,162] and have challenged the field to develop more rigorous quantitative methods.[163,164]

PO_2 MAPPING. The paramagnetic effects of oxygen reduce the T_1 and T_2 of HP gases (as well as proton signals)[2] and can therefore be exploited to provide a quantitative estimate of regional pO_2.[47,165,166] Typically, the same slice is imaged repeatedly at different delay times following gas inhalation to separate RF saturation of signal from signal loss due to local O_2 concentration.[167] The measurement is performed within a single breath-hold.[47,168] Modified centric and reverse-centric view orders mitigate effects due to locally variable flip angle (B_1-field variation).[168] Gas flow effects within the lungs during a breath-hold using ^{3}He have recently been described, underscoring that pO_2 is a mixture of regional pO_2 and local collateral ventilation effects.[169] Regional pO_2 measures can potentially be used to calculate the ratio of ventilation to perfusion (V/Q).[167] In fact, pO_2 measurements have recently been used as a marker of disease severity in a study of V/Q heterogeneity in smokers.[170,171]

^{129}XE MRI OF GAS EXCHANGE. The soluble "dissolved phase" fraction of ^{129}Xe in blood and tissues is ~2% of the

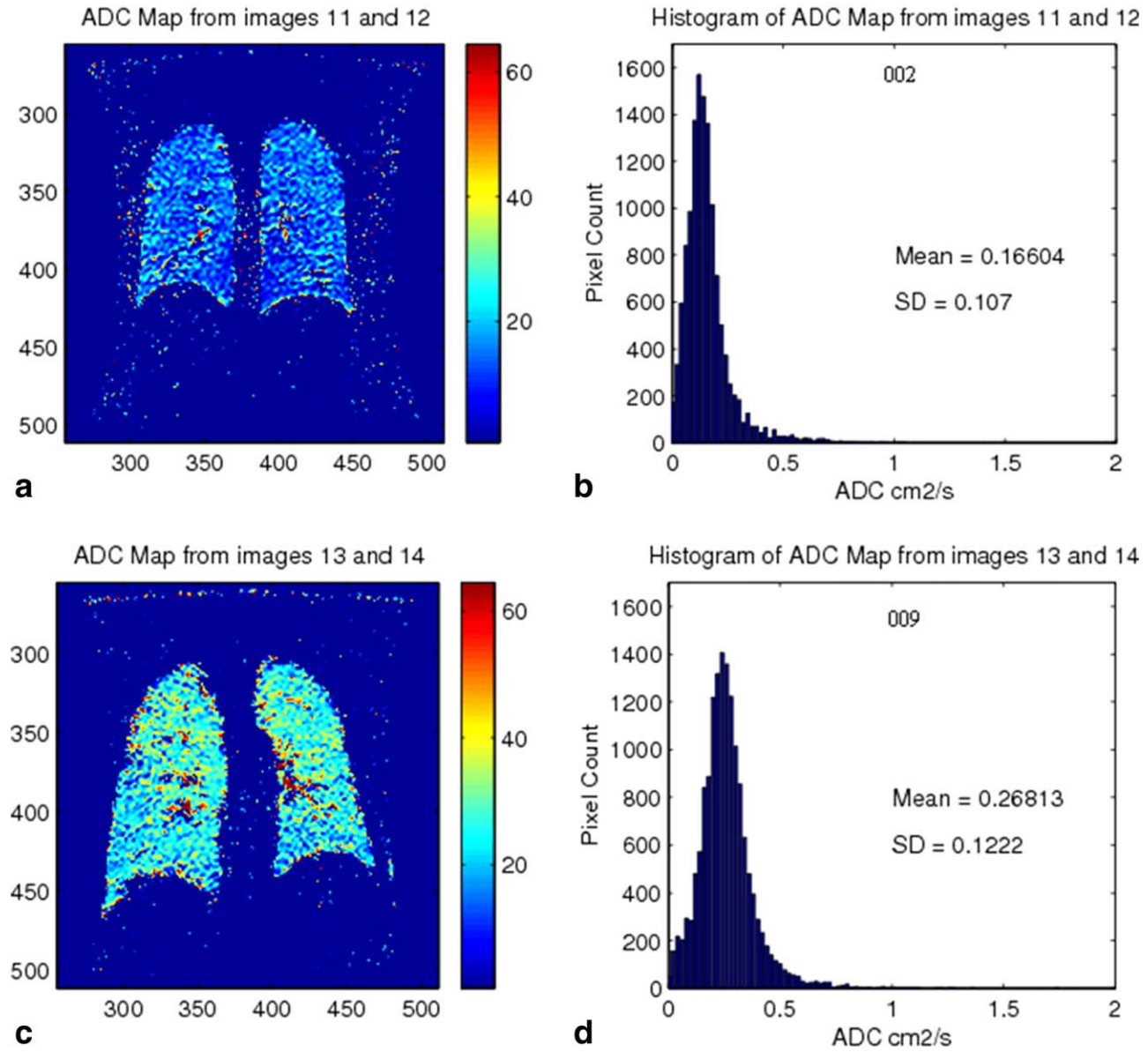

FIGURE 4: ADC maps derived from coronal slices acquired using diffusion-weighted ^{3}He MRI for (a) nonsmoker with (b) histogram for the typical slice shown, mean ADC = 0.166 cm^2/s and (c) smoker with (d) histogram mean ADC = 0.268 cm^2/s. Color bar units: mm^2/s. Adapted from Ref. 134 with permission.

total signal after accounting for the lower density of lung tissue and blood in the lungs. The dissolved phase of ^{129}Xe has a different chemical shift frequency than the gas phase. This fact can be exploited to quantify gas exchange. Polarized gas nuclei diffuse rapidly between gas, blood cells, and plasma/tissue compartments, with different chemical shifts in each compartment: 0 ppm, 222 ppm, and 198 ppm, respectively (Fig. 1).[172] Compartmental modeling of these components has advanced relatively rapidly.[173] Simple and robust single voxel MR spectroscopy readily resolves tissue and blood fractions and enables the calculation of blood/tissue ratio as a possible biomarker of diffusion block.[174,175] More quantitative measures such as saturation transfer time allow the kinetics of ^{129}Xe recovery to be modeled. These more advanced methods can provide direct[10,70,71,176] or indirect[72,73] estimates of average septal wall thickness and alveolar surface area to volume ratio.[72,173,177] Both single-voxel[177,178] and spectroscopic imaging methods[10,71] are feasible.

CLINICAL RESEARCH. The vast majority of clinical research studies using HP gas MRI have been performed in asthma[127,132,139,143,144,179,180] and COPD,[133,153,181] with a growing number of recent studies focusing on CF in children and adults.[142,182,183] Perhaps the greatest advantage of pulmonary MRI is for characterizing, or phenotyping, disease progression and severity. The ADC has found particular utility in studies of COPD that have shown that ADC correlates with pulmonary function,[153,184,185] is highly reproducible,[148] and is sensitive to subclinical disease[134–136,186] and disease progression.[150,181] A multi-institutional prospective study of COPD

in 122 subjects found that ADC was more predictive of COPD severity and more highly correlated with DLCO than quantitative CT.[131] In a separate 2-year longitudinal study of subjects with mild to moderate COPD, both ADC and VDP increased in the absence of significant change in FEV_1, suggesting progression detected by imaging but not conventional methods.[181] In mild to moderate COPD, the VDP in particular is associated with severe outcomes such as hospitalizations for exacerbations—an association that is not observed using conventional measures, including CT.[145] This work suggests the potential use of HP gas MRI to identify patients most likely to have severe outcomes at an earlier stage of disease progression. This, in turn, could allow more aggressive treatment to be targeted at these higher-risk individuals—an example of HP gas MRI providing the means to personalized medicine.[187]

In asthma, regional ventilation heterogeneity revealed by HP ^{3}He MRI has changed the way in which clinicians and researchers view this disease. Relatively large cross-sectional and longitudinal studies[141,143,188] have revealed that up to half of ventilation defects persist in the same locations over time intervals of several days to a year.[188] The persistence of ventilation defects in these studies was independent of asthma severity and medication use, suggesting that persistent defects were refractory to therapy. Because defects are observed even in asymptomatic patients and involve both the central and peripheral airways, conventional assumptions that asthma is a predominantly small airways disease have been challenged.[189–191] VDP and ADC-related measures are also associated with both differences in lung microstructure in asthma compared with controls[192] and also with asthma risk factors in adults[193,194] and children.[101,190]

Other important emerging applications using HP gas MRI include image-guided therapy, characterization of gas exchange, and combined structure-function MRI. Image-guided interventions using HP ^{3}He MRI show promise for evaluating the effects of stent placement in COPD,[28,195,196] smooth muscle ablation treatments in asthma,[27,197] and radiation treatment planning in lung cancer.[198–203] There will be a growing role for HP gas MRI in assessing the response to therapy and progression of disease in CF.[100,142,182,183] Moreover, gas exchange imaging with ^{129}Xe MRI shows promise for detection of gas diffusion block in idiopathic pulmonary fibrosis (IPF), a disease that is presently untreatable and for which conventional diagnostic imaging methods such as CT are insensitive.[175] However, with promising drug trials currently in progress early detection and prognosis may be sensitively detected with HP ^{129}Xe MRI.

Fluorinated Gases

IMAGES OF VENTILATION. The first use of fluorinated gas for lung ventilation MRI in vivo was in 1984 by Rinck et al[204] in a dog study. However, the technique was not widely adopted in research settings until the late 1990s. In 1998, Kuethe et al[3] demonstrated an early proof of principle experiment in a rat model using a 3D radial acquisition with C_2F_6. Image acquisition times were in excess of 4 hours to achieve an SNR of 8, but the 3D images were of good quality. In a reproducibility and validation pig study, Scholz et al[50] compared ventilation imaging with SF_6 with respiratory gas analysis by measuring the fluorine content of exhaled gas simultaneously. The reproducibility of both techniques was strong, with a standard error across 24 breaths of 8% for imaging and 5% for respiratory gas analysis. In addition, the expected correlation between the two techniques was very high ($R = 0.99$).

In the late 1990s and early 2000s, several groups[39,205,206] demonstrated that the paramagnetic effect of oxygen on the T_1 relaxation time of fluorinated gas made it possible to extrapolate the regional pO_2 using ^{19}F MRI. This work demonstrated the potential of regional assessment of lung physiology; a gravitational dependence of pO_2 opposite to that expected was observed,[39,207] with the ventral regions of the supine anesthetized pig exhibiting higher pO_2 compared to the dorsal regions.

In 2013 Carrero-Gonzalez et al[67] compared ADC values between 5 healthy normal rats and 6 rats that had undergone elastase treatment in one lung as a model of emphysema. ADC values in the control rats did not differ between right and left lungs. However, in the treated rats, ADC values were significantly higher in the elastase-treated lung compared to the normal lung. The ADC of the untreated lung did not differ from the control rats. In addition, elastase-treated lungs were more heterogeneous than normal lungs.

More recently, advanced MR acquisition schemes have enabled full 3D ventilation imaging in healthy human subjects. By implementing a 3D radial UTE FID sequence, Couch et al[87] were able to perform full 3D volumetric ventilation imaging in a 15-second breath-hold of C_3F_8. Image quality was quite good (Fig. 5), and a relatively homogeneous distribution of ventilation was observed. Importantly, SNR increased by nearly a factor of 2 when ^{19}F gas was allowed to wash into the lungs prior to imaging by breathing a mixture of O_2 and C_3F_8. This observation opened up the possibility of using the technique to assess fractional ventilation (defined as the ratio of fresh gas entering a volume "region" of the lung to the total end-inspiratory volume of the region[208]) by imaging dynamically.

The short T_1 recovery time of fluorinated gases combined with the use of equilibrium phase polarization allows repeated acquisitions over short temporal windows. Therefore, fluorinated gases are well suited for dynamic imaging of ventilation. The first feasibility study of dynamic fluorinated gas MRI was done in a pig model by Schreiber

et al.[51] They measured SF_6 washout time constants and demonstrated an inverse correlation between washout time and tidal volume. In a follow-up study, Wolf et al[52] demonstrated the feasibility of dynamic C_2F_6 MRI, also in a pig model. Although a direct comparison to SF_6 was beyond the scope of the work, high-quality dynamic images were demonstrated with a 2-second temporal resolution. In a rat study comparing SF_6 and C_3F_8 for the purpose of mapping regional fractional ventilation, Ouriadov et al[209] showed that while SF_6 baseline images had superior SNR, both gases yielded similar values for fractional ventilation. Moreover, a gravitational dependence of fractional ventilation was observed, in good agreement with previous results using nuclear imaging, HP gas MRI, and oxygen-enhanced (OE) MRI.[115,144,210,211]

DIFFUSION-WEIGHTED IMAGING (DWI). To mitigate the rapid T_2 and T_2* decay, radial FID sequences with short TE are most commonly employed for DWI with ^{19}F. The first example of this was a 2005 study, in which Perez-Sanchez et al[69] measured an average ADC of SF_6 in a pool of five rats as $2.22 * 10^{-6}$ m/s^2. In another study[68] the same group measured the impact of the relative concentration, or partial pressure, of SF_6 mixed with respiratory gases and demonstrated variations in the free diffusivity of the gas mixture. The expected anisotropy of diffusion was in agreement with previous studies.[154,212] Interestingly, ADC measured at FRC was not significantly different from the ADC measured at TLC. This result differed from previous ^{3}He results that showed that ADC increased with lung inflation volume.[213]

Carrero-Gonzalez et al[67] suggest that C_2F_6 is superior to SF_6 for DWI because the longer relaxation times of C_2F_6 (Table 2) allow the estimation of ADC using lower b-values and thus shorter TE and higher SNR. In addition, limitations on the measurable diffusion time imposed by the finite diffusion gradients and the shorter T_2 of SF_6 approach the unrestricted diffusion regime in the lungs, and may not fully probe the lung microstructure. Despite these challenges, Chang and Conradi[38] and Couch et al[214] have recently published findings that suggest that DWI with ^{19}F may be feasible in healthy human subjects.

V/Q MAPPING. Since fluorinated gases do not cross the alveolar wall to enter the blood, they cannot be used directly to measure gas exchange. For spin density imaging an approximately normoxic mixture of 80% fluorinated gas/20% O_2 is typically used to maximize the number of fluorine spins per unit volume, albeit with an overall higher density than air. However, in preclinical studies Kuethe et al[88] presented an indirect method of estimating gas exchange with fluorinated gases. Regional pO_2 variations indirectly affect partial pressure of SF_6 because O_2 is taken up differentially in lung tissues and blood due to regional variations in ventilation (V) and perfusion (Q). Thus, steady-state images of fluorinated gas will show higher spin density in regions of high perfusion where oxygen is being rapidly removed and lower spin density in regions of reduced perfusion where higher pO_2 exists. Kuethe et al recognized that this effect is enhanced while breathing a hyperoxic gas mixture of fluorinated gas, eg, 30% SF_6/70% O_2, compared to a normoxic mixture, eg, 80% SF_6/20% O_2. Since the normoxic mixture is comparatively insensitive to V/Q, it can be used to normalize the hyperoxic image to remove physical variations related to the image acquisition, like B_1-field and coil sensitivity differences. Therefore, a ratio of the hyperoxic image to the normoxic image is proportional to regional V/Q (Fig. 6). This approach was refined by Adolphi and Kuethe[215] to obtain the V/Q estimate using the positive linear relationship between SF_6 partial pressure and local T_1 with a Look–Locker sequence. T_1 images were acquired with the hyperoxic mixture, 30% SF_6/70% O_2, alone. This method combines the tendency of SF_6 to gather in regions of poor V/Q matching with quantitative T_1 mapping that varies directly with SF_6 partial pressure and does not require a normoxic reference scan. Good agreement was shown between this T_1-mapping method and the original Kuethe et al technique.[88]

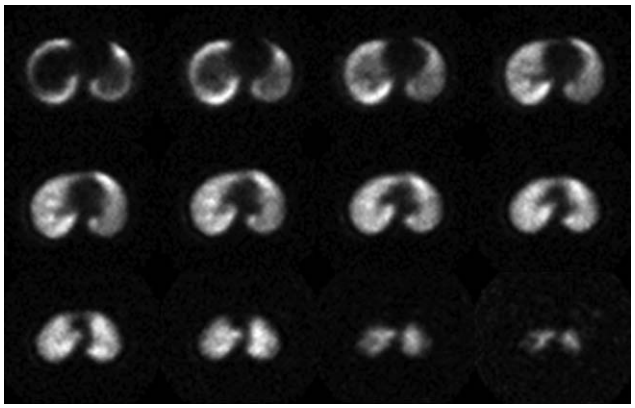

FIGURE 5: Axial reformation of 3D radial UTE FID MRI ventilation imaging with C_3F_8. This dataset was acquired in a 15-second breath-hold. Good image quality and the expected homogeneity of gas distribution are observable in this healthy normal human subject. Republished from Ref. 87 with permission.

CLINICAL RESEARCH. Overall, ^{19}F MRI is less well developed than HP gas MRI, likely due to the challenges with respect to development of gas delivery systems and SNR. Nonetheless, as the costs and access to HP gases have become increasingly challenging, there has been a revitalization of clinical research in this area. Compared to DWI using HP gas MRI methods that have been used successfully to demonstrate microstructural differences in subclinical and clinical obstructive lung disease, studies of DWI with fluorinated gases have been limited thus far to pre-clinical and ex vivo studies. In a study comparing ^{3}He MRI and ^{19}F MRI techniques, Conradi et al[38] demonstrated an increased mean

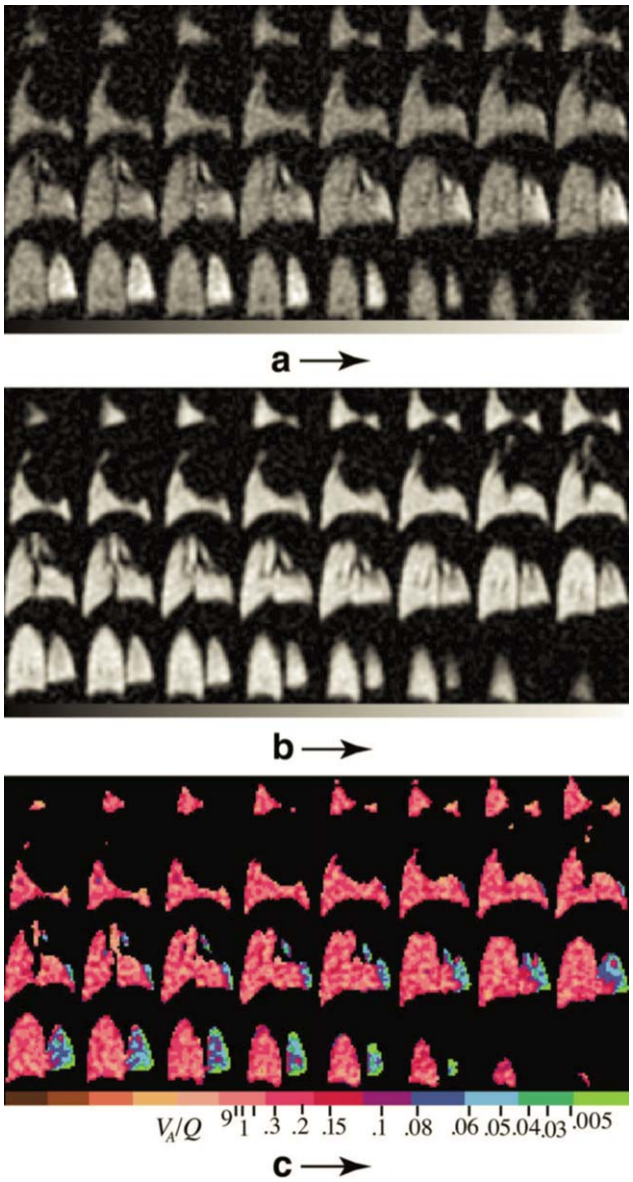

FIGURE 6: SF_6 MRI as a surrogate for V/Q measurement in a rat model of ventilation obstruction (left upper lobe). Multiple slices of a 3D volume acquired with the hyperoxic 30% SF_6/70% O_2 mixture (numerator) (a), and normoxic 80% SF_6/20% O_2 mixture (denominator) (b), and resulting ratio images (c). The color bars of the corresponding V/Q scale are the width of the SD of the ratio values. Republished from Ref. 215 with permission of the Journal of Magnetic Resonance in Medicine.

ADC of C_3F_8 in eight excised emphysematous human lungs compared to two excised normal donor lungs. In another study comparing healthy and emphysematous explanted lungs, Jacob et al[216] also demonstrated a higher ADC of C_2F_6 in the emphysematous lungs (0.018 cm/s^2 vs. 0.031 cm/s^2).

Preliminary studies of ventilation in human subjects by Halaweish et al[49] were performed in a range of patients with obstructive lung diseases. In all, 28 subjects were imaged (11 normal, two asthma, seven COPD, three transplant, one COPD/transplant, four emphysema) using 2D FLASH MRI with C_3F_8 to evaluate the suitability of ^{19}F breath-hold MRI for characterization of disease. Normal subjects demonstrated the expected homogeneous distribution of ^{19}F gas, while diseased subjects showed heterogeneity patterns that varied based on disease. As expected from previous studies with HP gas MRI, COPD subjects demonstrated ventilation defects that worsened with increasing disease severity. Asthmatic subjects did not present with ventilation defects, but the distribution of ^{19}F signal was significantly more heterogeneous than in healthy normal subjects. In a bronchiolitis obliterans subject with sibling donor transplant, it was possible to clearly differentiate the well-ventilated and homogeneous distribution of the healthy transplanted lung from the diseased lung, which demonstrated marked heterogeneity and ^{19}F ventilation defects (Fig. 7).

Ultimately, the promise of fluorinated gases are related to their relatively low cost, the avoidance of complex hyperpolarization hardware, the ability to image during steady-state breathing, a resonance frequency very close to proton resonance frequency, and a relatively high SNR (albeit lower than with HP gases). The very short T_1 of ^{19}F compounds allows dynamic imaging that can be used to provide more quantitative ventilation measures including estimates of V/Q. The confirmation of heterogeneity and ventilation defects in disease, DWI anisotropy, and gravitational dependences previously seen with HP gas MRI makes ^{19}F MRI a promising approach, with potential for clinical translation. The image quality of ^{19}F approaches is lower than HP gas MRI, although it continues to improve and may eventually prove an attractive alternative to HP gas MRI.

Oxygen Enhanced

STEADY-STATE IMAGING. The first breath-held OE-MRI images were described by Edelman et al,[2] acquired with an IR-SSFSE sequence. Oxygen-enhanced signal is observable in the regions corresponding to healthy lung (Fig. 8), while regions corresponding to bullous emphysema have a markedly lower signal enhancement. In an animal model, Chen et al[114] demonstrated ventilation-perfusion matching of abnormalities comparing OE-MRI to contrast-enhanced perfusion MRI by occluding a secondary bronchus using a balloon catheter. Dietrich et al[85] demonstrated an effective multislice OE-MRI acquisition in healthy human subjects through the use of interleaved slices, dual respiratory and cardiac gating, and parallel imaging. In 2014, Kruger et al[11] demonstrated the feasibility of 3D isotropic OE-MRI using a 3D radial UTE sequence in healthy human subjects (Fig. 9).

DYNAMIC IMAGING. The first publication that reported wash-in and washout decay constants by using dynamic OE MRI was by Hatabu and colleagues.[81] Subjects were

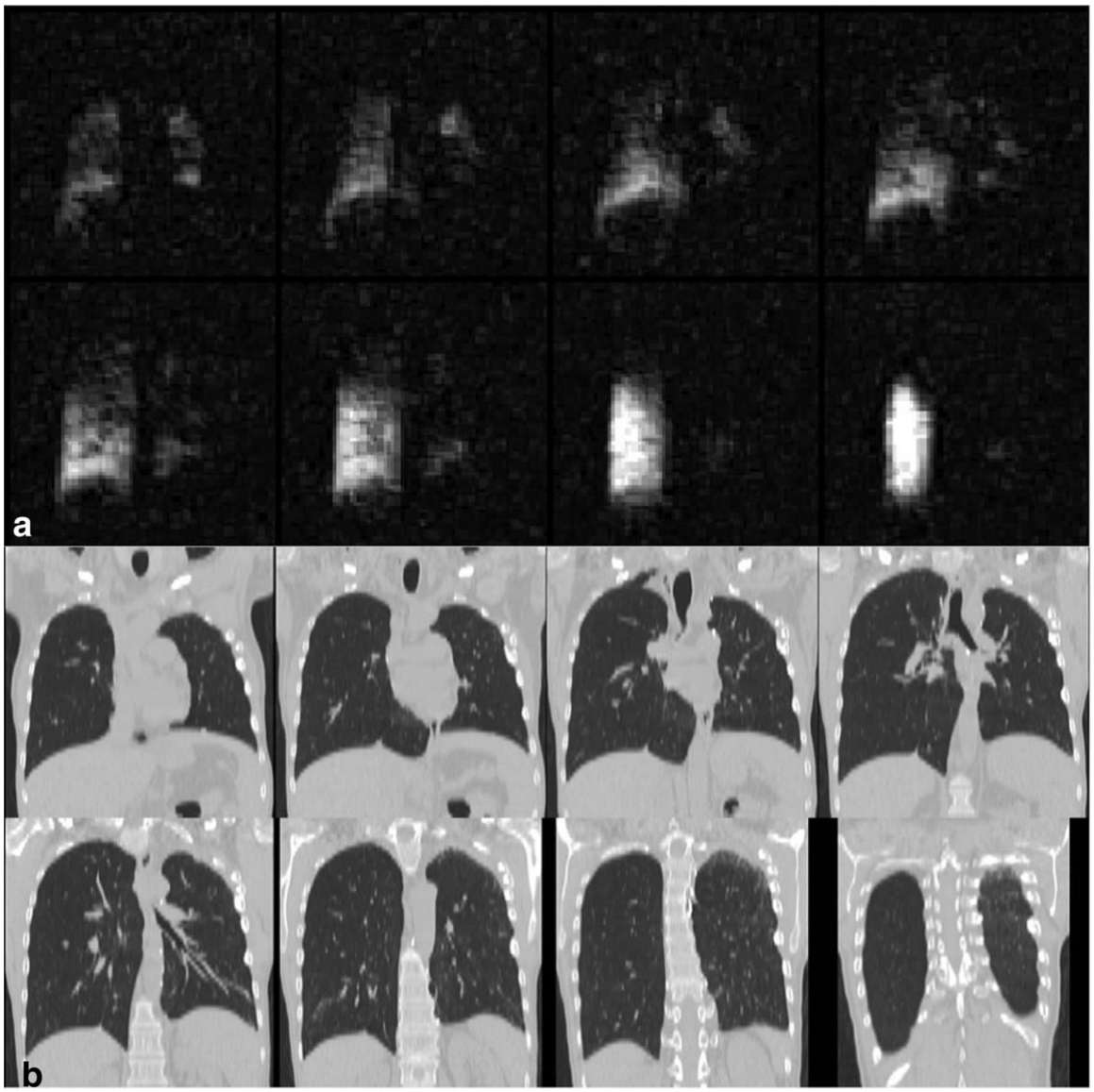

FIGURE 7: (a) ventilation image of a lung transplant recipient (coronal field of view 40 cm). Prior to this study, both lungs had developed BOS after transplant from a nonsibling donor. The right lung was then transplanted from a sibling donor. The high ^{19}F signal intensity in the healthy right lung is clearly differentiable from the BOS left lung. (b) Matching CT slices (coronal field of view ~34 cm) to provide structural reference. Republished from Ref. 49 with permission.

scanned using an IR-SSFSE sequence. Acquisition was respiratory gated to end-expiration and an image was acquired every 3 seconds as the FiO_2 was varied. Dynamic 2D OE MRI images were acquired by averaging of SSFSE images over a moving temporal averaging window and calculating PSE relative to baseline. Dynamic signal in an ROI was fit to an exponential curve to calculate decay constants of ~20–25 seconds for O_2 wash-in and washout. Successive works by Ohno et al[107,217] with dynamic OE MRI found a correlation of PSE with diffusing capacity $\%DL_{CO}$. In addition, the oxygen wash-in time was shown to correlate inversely with $\%DL_{CO}$ and FEV_1. Sa et al[115] and Tedjasaputra et al[218] used a similar technique for a voxelwise computation of specific ventilation (SV)[219] using OE MRI, and showed the well-known gravitational dependence[207,220] in SV using this method. Dynamic acquisition of T_1 maps during oxygen wash-in and washout to obtain regional time constants of R1 ($=1/T_1$) has also been explored as a quantitative marker of lung function.[79]

CLINICAL RESEARCH. Ohno et al[81] showed in a 2001 study that mean PSE in 10 cancer subjects was lower than that in seven healthy normal subjects, while the combination of cancer and emphysema in eight subjects resulted in an even lower PSE. In an effort to segment localized ventilation defects, Nakagawa et al[221] in 2001 compared OE MRI and contrast-enhanced perfusion MRI in nine cancer and six pulmonary embolism (PE) subjects. The typical ventilation-perfusion mismatch expected in PE was observed. No ventilation defects were found in either case,

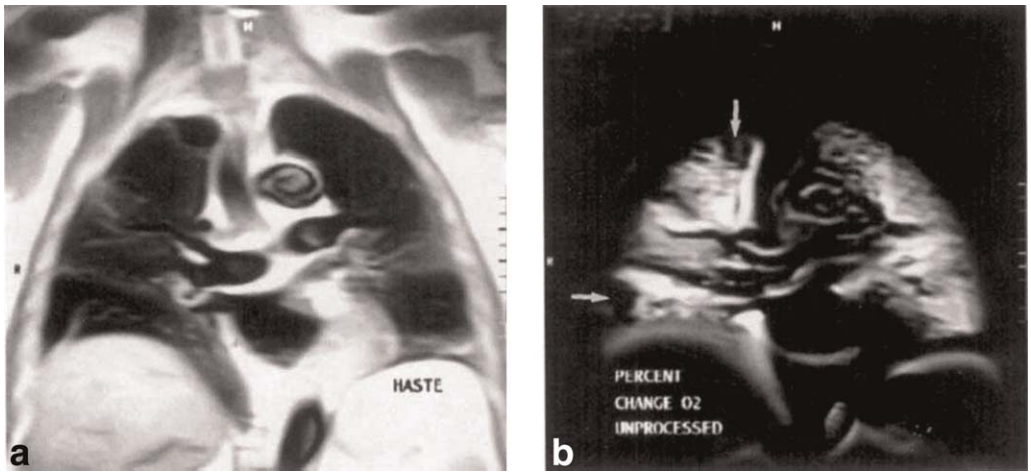

FIGURE 8: (a) Coronal IR-SSFSE image showing low-signal regions in the right lung corresponding to bullae. (b) OE MRI showing ventilation defects (arrows) in the bullous regions. Originally published in Ref. 2, reprinted with the permission of Nature Medicine.

even in the regions of clear perfusion defect shown on perfusion MRI. In a 2005 study of 30 cancer subjects, Ohno et al[222] demonstrated that OE-MRI was equal or superior to CT and nuclear scintigraphy in predicting postsurgical lung function as measured by FEV_1.

In 2004, Jakob et al[78] measured the OTF directly in a pool of five normal and five CF subjects by repeating T_1 measurements at various FiO_2 using an IR-FLASH sequence. In normal subjects they found a homogeneous distribution of T_1 under normoxic conditions, and a homogeneous decrease in T_1 under hyperoxic conditions. However, CF subjects showed an inhomogeneous distribution of T_1 under normoxic conditions. Under hyperoxic conditions the diseased lung regions (as measured with perfusion MRI) had a smaller OE-related decrease in T_1 than the more normal lung regions. In 2014, Kruger[223] demonstrated significant correlation between ventilation defects in CF as measured with 3D radial UTE OE MRI and HP ^{3}He MRI (Fig. 10).

Ohno et al[217,224] have found that PSE on OE MRI is lower and more heterogeneous in emphysema subjects compared to healthy normal subjects. In addition, a later trial comparing PSE as measured with OE MRI to functional lung volume (FLV) as measured with CT[225] in a pool of 160 smokers showed that OE MRI yielded a superior correlation coefficient to pulmonary function tests. Furthermore, PSE as measured with OE MRI correlated with disease severity classifications for emphysema.

Using dynamic OE MRI, the oxygen wash-in slope was found to inversely correlate with $\%DL_{CO}$ in smoking-related COPD[107] and IPF.[83] In a small study of mild/moderate and severe asthma, reduced oxygen wash-in time constant and mean peak enhancement were associated with greater severity.[32] In addition, in studies of lung volume reduction surgery candidates[226] and asthma patients,[227,228] OE MRI showed equal or superior performance in detecting treatment effect and disease severity compared with PFT, CT, and/or nuclear medicine study. More recently the OTF was shown to decrease in asthmatics after allergen challenge and correlated with the percentage of eosinophils in bronchoalveolar lavage at the site of challenge.[229]

The ready availability of oxygen and the freedom from dedicated multinuclear imaging hardware make OE MRI a

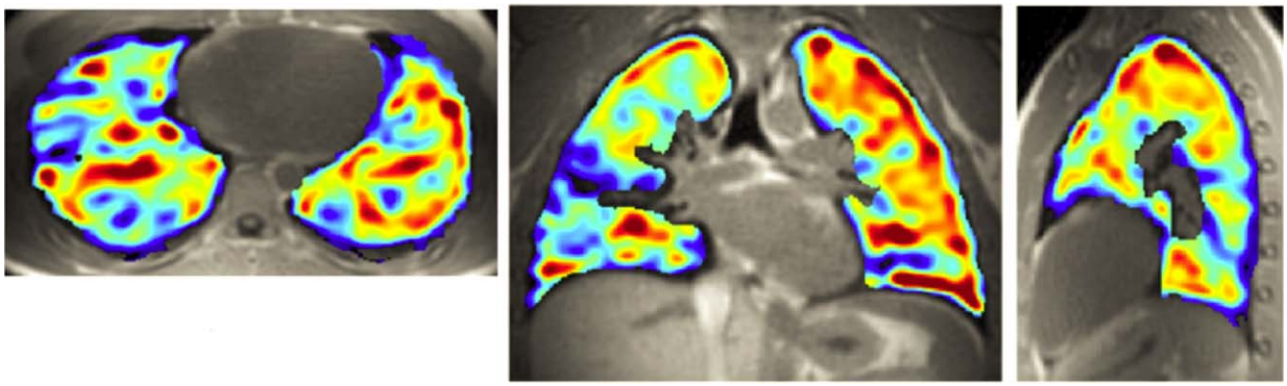

FIGURE 9: Example from Ref. 11 showing a healthy normal subject with parametric color map. The isotropic 3D resolution is apparent in the axial, coronal, and sagittal reformations of the same dataset. The color bar is in units of percent signal enhancement (PSE).

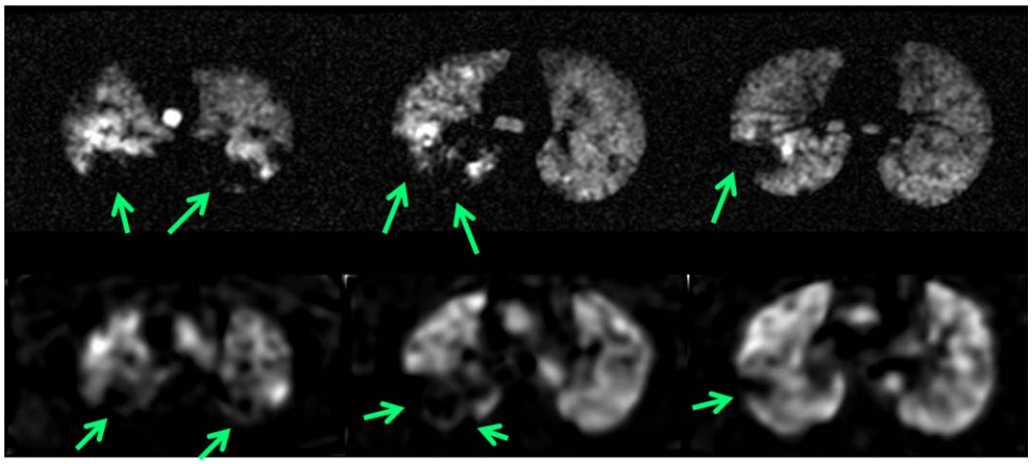

FIGURE 10: Comparison of HP ^{3}He MRI images (top row) with OE-MRI images (bottom row) originally presented in Ref. 223. Arrows indicate regions of agreement in ventilation defect extent and location. The in-plane spatial resolution of the HP ^{3}He images is greater than in the OE MRI images by a factor of 3.2. However, the resolution in the OE MRI images in this study was isotropic in all three dimensions, while the HP ^{3}He images were anisotropic with 1 cm thick axial slices.

promising research tool with high potential for clinical translation. The technique has shown strong correlations with other reference standards for pulmonary function such as PFT, CT, DLCO, scintigraphy, and HP ^{3}He MRI. Before OE MRI will be able to move into routine clinical use, however, further work with respect to quantitative analysis and reproducibility of the various OE MRI metrics is needed.

Discussion

As shown in Table 3, the current and emerging pulmonary functional MRI methods each have significant strengths and challenges. Of the functional imaging techniques reviewed here, HP gases are more mature in their development, and therefore are better positioned for short-term clinical success. However, limited cost and access to HP gases has led directly to the recent efforts to advance fluorinated and oxygen-enhanced MRI, which could change the cost–benefit tradeoffs currently slowing dissemination of FLI methods to the clinic.

Pulmonary MRI approaches have important advantages over established clinical methods such as pulmonary function testing and scintigraphy that could change the current cost–benefit calculus. Pulmonary function testing cannot easily characterize different phenotypes of disease. Furthermore, pulmonary function testing is a global assessment of the lungs and is generally insensitive to clinically important changes in disease severity that might impact patient management, especially as more therapy options become available and more mild disease is targeted. The spatial resolution of scintigraphy is generally poorer than that achievable with MRI and scintigraphy requires ionizing radiation. The use of x-ray-based methods, including CT, diminish the numbers and types of imaging sessions that are practical for longitudinal assessment of lung disease due to the potentially harmful effects of accumulated ionizing radiation exposure in patients with chronic lung disease. The continued development of ultra-low dose CT[230] may impact this assessment, but it should also be noted that newer FLI methods using x-ray CT—for example, perfusion[231] and dual energy xenon CT[232]—require more radiation than standard chest CT. Furthermore, recent advances in gradient performance and image reconstruction have significantly improved image quality for structural MRI of the lungs. This has led to advances in combined structure–function assessment of disease severity and therapy response in CF only possible with pulmonary MRI.[233]

There remain significant challenges to translating FLI methods to the clinic. Unlike many organ systems where early or sensitive diagnosis has led to earlier and efficacious treatments, this virtuous cycle is only now emerging for many respiratory diseases. Nonetheless, respiratory diseases still have significant unmet needs in terms of pharmaceutical development, minimally invasive interventions, longitudinal follow-up, and prognosis. Disorders such as asthma and COPD are widespread and will continue to be a leading cause of death and disease as the world becomes more industrialized and polluted. The gas agents reviewed here underscore the unique ability of pulmonary MRI to measure the functional consequences of obstructive lung diseases. Moreover, continued dissemination and advances in UTE MRI further support an emerging clinical role for combined structure–function imaging. Complementary approaches that use the gas and technique best suited to the available hardware capabilities of a given site may become feasible as the field and clinical research community matures.

References

1. Hatabu H, Alsop DC, Listerud J, Bonnet M, Gefter WB. T2* and proton density measurement of normal human lung parenchyma using submillisecond echo time gradient echo magnetic resonance imaging. Eur J Radiol 1999;29:245–252.

2. Edelman RR, Hatabu H, Tadamura E, Li W, Prasad PV. Noninvasive assessment of regional ventilation in the human lung using oxygen-enhanced magnetic resonance imaging. Nat Med 1996;2:1236–1239.
3. Kuethe DO, Caprihan A, Fukushima E, Waggoner RA. Imaging lungs using inert fluorinated gases. Magn Reson Med 1998;39:85–88.
4. Fain S, Schiebler ML, McCormack DG, Parraga G. Imaging of lung function using hyperpolarized helium-3 magnetic resonance imaging: Review of current and emerging translational methods and applications. J Magn Reson Imaging JMRI 2010;32:1398–1408.
5. Mugler JP 3rd, Altes TA. Hyperpolarized 129Xe MRI of the human lung. J Magn Reson Imaging JMRI 2013;37:313–331.
6. Pruessmann KP, Weiger M, Scheidegger MB, Boesiger P. SENSE: sensitivity encoding for fast MRI. Magn Reson Med 1999;42:952–962.
7. Griswold MA, Jakob PM, Heidemann RM, et al. Generalized autocalibrating partially parallel acquisitions (GRAPPA). Magn Reson Med 2002;47:1202–1210.
8. Lustig M, Donoho D, Pauly JM. Sparse MRI: the application of compressed sensing for rapid MR imaging. Magn Reson Med 2007;58: 1182–1195.
9. Mistretta CA, Wieben O, Velikina J, et al. Highly constrained backprojection for time-resolved MRI. Magn Reson Med 2006;55:30–40.
10. Qing K, Ruppert K, Jiang Y, et al. Regional mapping of gas uptake by blood and tissue in the human lung using hyperpolarized xenon-129 MRI. J Magn Reson Imaging JMRI 2014;39:346–359.
11. Kruger SJ, Fain SB, Johnson KM, Cadman RV, Nagle SK. Oxygen-enhanced 3D radial ultrashort echo time magnetic resonance imaging in the healthy human lung. NMR Biomed 2014;27:1535–1541.
12. Bauman G, Johnson KM, Bell LC, et al. Three-dimensional pulmonary perfusion MRI with radial ultrashort echo time and spatial-temporal constrained reconstruction. Magn Reson Med 2015;73:555–564.
13. Bianchi A, Ozier A, Ousova O, Raffard G, Cremillieux Y. Ultrashort-TE MRI longitudinal study and characterization of a chronic model of asthma in mice: inflammation and bronchial remodeling assessment. NMR Biomed 2013;26:1451–1459.
14. Togao O, Ohno Y, Dimitrov I, Hsia CC, Takahashi M. Ventilation/perfusion imaging of the lung using ultra-short echo time (UTE) MRI in an animal model of pulmonary embolism. J Magn Reson Imaging JMRI 2011;34:539–546.
15. Johnson KM, Fain SB, Schiebler ML, Nagle S. Optimized 3D ultrashort echo time pulmonary MRI. Magn Reson Med 2013;70:1241–1250.
16. Weiger M, Pruessmann KP, Hennel F. MRI with zero echo time: hard versus sweep pulse excitation. Magn Reson Med 2011;66:379–389.
17. Grodzki DM, Jakob PM, Heismann B. Ultrashort echo time imaging using pointwise encoding time reduction with radial acquisition (PETRA). Magn Reson Med 2012;67:510–518.
18. Bieri O. Ultra-fast steady state free precession and its application to in vivo H morphological and functional lung imaging at 1.5 Tesla. Magn Reson Med 2013;70:657–663.
19. Miller GW, Mugler JP 3rd, Sa RC, Altes TA, Prisk GK, Hopkins SR. Advances in functional and structural imaging of the human lung using proton MRI. NMR Biomed 2014;27:1542–1556.
20. Levitsky MG. Pulmonary physiology. New York: McGraw-Hill; 2007.
21. Sorkness RL, Bleecker ER, Busse WW, et al. Lung function in adults with stable but severe asthma: air trapping and incomplete reversal of obstruction with bronchodilation. J Appl Physiol 2008;104:394–403.
22. Hankinson JL, Odencrantz JR, Fedan KB. Spirometric reference values from a sample of the general U.S. population. Am J Respir Crit Care Med 1999;159:179–187.
23. Quanjer PH, Stanojevic S, Cole TJ, et al. Multi-ethnic reference values for spirometry for the 3-95-yr age range: the global lung function 2012 equations. Eur Respir J 2012;40:1324–1343.
24. Crapo RO, Gardner RM. DLCO reference equations: a perspective. Am Rev Respir Dis 1986;134:856.
25. Gustafsson PM, De Jong PA, Tiddens HA, Lindblad A. Multiple-breath inert gas washout and spirometry versus structural lung disease in cystic fibrosis. Thorax 2008;63:129–134.
26. Castro M, Cox G. Asthma outcomes from bronchial thermoplasty in the AIR2 trial. Am J Respir Crit Care Med 2011;184:743–744.
27. Thomen RP, Sheshadri A, Quirk JD, et al. Regional ventilation changes in severe asthma after bronchial thermoplasty with (3)He MR imaging and CT. Radiology 2015;274:250–259.
28. Mata J, Altes T, Truwit J, et al. Characterization and detection of physiologic lung changes before and after placement of bronchial valves using hyperpolarized helium-3 MR imaging: preliminary study. Acad Radiol 2011;18:1195–1199.
29. Melo V. Quantification of regional ventilation-perfusion ratios with PET. J Nucl Med 2003;44:1982–1991.
30. Bauman G, Eichinger M. Ventilation and perfusion magnetic resonance imaging of the lung. Pol J Radiol 2012;77:37–46.
31. Kuo W, Ciet P, Tiddens H, Zhang W, Guillerman RP, van Straten M. Reply: cumulative radiation exposure to abdominal organs in patients with cystic fibrosis should not be forgotten. Am J Respir Crit Care Med 2014;190:962.
32. Kuo W, Ciet P, Tiddens HA, Zhang W, Guillerman RP, van Straten M. Monitoring cystic fibrosis lung disease by computed tomography. Radiation risk in perspective. Am J Respir Crit Care Med 2014;189: 1328–1336.
33. de Jong PA, Tiddens HA, Lequin MH, Robinson TE, Brody AS. Estimation of the radiation dose from CT in cystic fibrosis. Chest 2008; 133:1289–1291; author reply 1290–1291.
34. Bouchiat MA, Carver TR, Varnum CM. Nuclear polarisation in 3He gas induced by optical pumping and dipolar exchange. Phys Rev Lett 1960;5:373–375.
35. Happer W, Miron E, Schaefer D, Schreiber WA, van Wijngaarden A, Zeng X. Polarization of the nuclear spins of noble-gas atoms by spin exchange with optically pumped alkali-metal atoms. Am Phys Soc 1984;29:3092–3110.
36. Walker TG, Happer W. Spin-exchange optical pumping of noble-gas nuclei. Rev Mod Phys 1997;69:629–642.
37. Ruiz-Cabello J, Barnett BP, Bottomley PA, Bulte JW. Fluorine (19F) MRS and MRI in biomedicine. NMR Biomed 2011;24:114–129.
38. Chang YV, Conradi MS. Relaxation and diffusion of perfluorocarbon gas mixtures with oxygen for lung MRI. J Magn Reson 2006;181:191–198.
39. Laukemper-Ostendorf S, Scholz A, Burger K, et al. 19F-MRI of perflubron for measurement of oxygen partial pressure in porcine lungs during partial liquid ventilation. Magn Reson Med 2002;47:82–89.
40. de Lange EE, Mugler JP 3rd, Brookeman JR, et al. Lung air spaces: MR imaging evaluation with hyperpolarized 3He gas. Radiology 1999; 210:851–857.
41. Wild JM, Paley MN, Viallon M, Schreiber WG, van Beek EJ, Griffiths PD. k-space filtering in 2D gradient-echo breath-hold hyperpolarized 3He MRI: spatial resolution and signal-to-noise ratio considerations. Magn Reson Med 2002;47:687–695.
42. Wild JM, Woodhouse N, Paley MN, et al. Comparison between 2D and 3D gradient-echo sequences for MRI of human lung ventilation with hyperpolarized 3He. Magn Reson Med 2004;52:673–678.
43. Holmes JH, O'Halloran RL, Brodsky EK, Jung Y, Block WF, Fain SB. 3D hyperpolarized He-3 MRI of ventilation using a multi-echo projection acquisition. Magn Reson Med 2008;59:1062–1071.
44. Wild JM, Paley MN, Kasuboski L, et al. Dynamic radial projection MRI of inhaled hyperpolarized 3He gas. Magn Reson Med 2003;49:991–997.
45. Zhao L, Albert MS. Biomedical imaging using hyperpolarized noble gas MRI: pulse sequence considerations. Nucl Instrum Methods Phys Research A 1998;402:454–460.
46. Wild JM, Teh K, Woodhouse N, et al. Steady-state free precession with hyperpolarized 3He: experiments and theory. J Magn Reson 2006;183:13–24.

47. Fischer MC, Spector ZZ, Ishii M, et al. Single-acquisition sequence for the measurement of oxygen partial pressure by hyperpolarized gas MRI. Magn Reson Med 2004;52:766–773.

48. Horn FC, Deppe MH, Marshall H, Parra-Robles J, Wild JM. Quantification of regional fractional ventilation in human subjects by measurement of hyperpolarized 3He washout with 2D and 3D MRI. J Appl Physiol 2014;116:129–139.

49. Halaweish AF, Moon RE, Foster WM, et al. Perfluoropropane gas as a magnetic resonance lung imaging contrast agent in humans. Chest 2013;144:1300–1310.

50. Scholz AW, Wolf U, Fabel M, et al. Comparison of magnetic resonance imaging of inhaled SF6 with respiratory gas analysis. Magn Reson Imaging 2009;27:549–556.

51. Schreiber WG, Eberle B, Laukemper-Ostendorf S, et al. Dynamic (19)F-MRI of pulmonary ventilation using sulfur hexafluoride (SF(6)) gas. Magn Reson Med 2001;45:605–613.

52. Wolf U, Scholz A, Heussel CP, Markstaller K, Schreiber WG. Subsecond fluorine-19 MRI of the lung. Magn Reson Med 2006;55:948–951.

53. Salerno M, Altes TA, Brookeman JR, de Lange EE, Mugler JP 3rd. Dynamic spiral MRI of pulmonary gas flow using hyperpolarized (3)He: preliminary studies in healthy and diseased lungs. Magn Reson Med 2001;46:667–677.

54. Holmes JH, O'Halloran RL, Brodsky EK, et al. Three-dimensional imaging of ventilation dynamics in asthmatics using multiecho projection acquisition with constrained reconstruction. Magn Reson Med 2009;62:1543–1556.

55. O'Halloran RL, Holmes JH, Wu YC, Alexander A, Fain SB. Helium-3 MR q-space imaging with radial acquisition and iterative highly constrained back-projection. Magn Reson Med 2010;63:41–50.

56. Ajraoui S, Parra-Robles J, Wild JM. Incorporation of prior knowledge in compressed sensing for faster acquisition of hyperpolarized gas images. Magn Reson Med 2013;69:360–369.

57. Stewart NJ, Norquay G, Griffiths PD, Wild JM. Feasibility of human lung ventilation imaging using highly polarized naturally abundant xenon and optimized three-dimensional steady-state free precession. Magn Reson Med 2015 [Epub ahead of print].

58. Lee RF, Johnson G, Grossman RI, Stoeckel B, Trampel R, McGuinness G. Advantages of parallel imaging in conjunction with hyperpolarized helium—a new approach to MRI of the lung. Magn Reson Med 2006; 55:1132–1141.

59. Dregely I, Ruset IC, Wiggins G, et al. 32-channel phased-array receive with asymmetric birdcage transmit coil for hyperpolarized xenon-129 lung imaging. Magn Reson Med 2013;70:576–583.

60. Emami K, Xu Y, Hamedani H, et al. Accelerated fractional ventilation imaging with hyperpolarized Gas MRI. Magn Reson Med 2013;70: 1353–1359.

61. Kadlecek S, Hamedani H, Xu Y, et al. Regional alveolar partial pressure of oxygen measurement with parallel accelerated hyperpolarized gas MRI. Acad Radiol 2013;20:1224–1233.

62. MacDonald A, Wann K. Physiologic aspects of anaesthetics and inert gases. London: Academic Press; 1978.

63. Chen XJ, Moller HE, Chawla MS, et al. Spatially resolved measurements of hyperpolarized gas properties in the lung in vivo. Part II: T *(2). Magn Reson Med 1999;42:729–737.

64. Saam BT, Yablonskiy DA, Kodibagkar VD, et al. MR imaging of diffusion of (3)He gas in healthy and diseased lungs. Magn Reson Med 2000;44:174–179.

65. Narayanan M, Owers-Bradley J, Beardsmore CS, et al. Alveolarization continues during childhood and adolescence: new evidence from helium-3 magnetic resonance. Am J Respir Crit Care Med 2012;185: 186–191.

66. Yablonskiy DA, Sukstanskii AL, Quirk JD, Woods JC, Conradi MS. Probing lung microstructure with hyperpolarized noble gas diffusion MRI: theoretical models and experimental results. Magn Reson Med 2014;71:486–505.

67. Carrero-Gonzalez L, Kaulisch T, Stiller D. In vivo diffusion-weighted MRI using perfluorinated gases: ADC comparison between healthy and elastase-treated rat lungs. Magn Reson Med 2013;70:1761–1764.

68. Ruiz-Cabello J, Perez-Sanchez JM, Perez de Alejo R, et al. Diffusion-weighted 19F-MRI of lung periphery: influence of pressure and air-SF6 composition on apparent diffusion coefficients. Respir Physiol Neurobiol 2005;148:43–56.

69. Perez-Sanchez JM, Perez de Alejo R, Rodriguez I, Cortijo M, Peces-Barba G, Ruiz-Cabello J. In vivo diffusion weighted 19F MRI using SF6. Magn Reson Med 2005;54:460–463.

70. Kaushik SS, Freeman MS, Cleveland ZI, et al. Probing the regional distribution of pulmonary gas exchange through single-breath gas- and dissolved-phase 129Xe MR imaging. J Appl Physiol 2013;115:850–860.

71. Qing K, Mugler JP 3rd, Altes TA, et al. Assessment of lung function in asthma and COPD using hyperpolarized (129) Xe chemical shift saturation recovery spectroscopy and dissolved-phase MRI. NMR Biomed 2014;27:1490–1501.

72. Ruppert K, Brookeman JR, Hagspiel KD, Mugler JP 3rd. Probing lung physiology with xenon polarization transfer contrast (XTC). Magn Reson Med 2000;44:349–357.

73. Dregely I, Mugler JP 3rd, Ruset IC, et al. Hyperpolarized Xenon-129 gas-exchange imaging of lung microstructure: first case studies in subjects with obstructive lung disease. J Magn Reson Imaging JMRI 2011;33:1052–1062.

74. Hatabu H, Tadamura E, Chen Q, et al. Pulmonary ventilation: dynamic MRI with inhalation of molecular oxygen. Eur J Radiol 2001;37:172–178.

75. Pracht ED, Arnold JF, Wang T, Jakob PM. Oxygen-enhanced proton imaging of the human lung using T2. Magn Reson Med 2005;53: 1193–1196.

76. Ogawa S, Lee TM, Kay AR, Tank DW. Brain magnetic resonance imaging with contrast dependent on blood oxygenation. Proc Natl Acad Sci U S A 1990;87:9868–9872.

77. Jakob PM, Hillenbrand CM, Wang T, Schultz G, Hahn D, Haase A. Rapid quantitative lung (1)H T(1) mapping. J Magn Reson Imaging JMRI 2001;14:795–799.

78. Jakob PM, Wang T, Schultz G, Hebestreit H, Hebestreit A, Hahn D. Assessment of human pulmonary function using oxygen-enhanced T(1) imaging in patients with cystic fibrosis. Magn Reson Med 2004; 51:1009–1016.

79. Arnold JF, Fidler F, Wang T, Pracht ED, Schmidt M, Jakob PM. Imaging lung function using rapid dynamic acquisition of T1-maps during oxygen enhancement. Magma 2004;16:246–253.

80. Stock KW, Chen Q, Morrin M, Hatabu H, Edelman RR. Oxygen-enhanced magnetic resonance ventilation imaging of the human lung at 0.2 and 1.5 T. J Magn Reson Imaging JMRI 1999;9:838–841.

81. Ohno Y, Hatabu H, Takenaka D, Adachi S, Van Cauteren M, Sugimura K. Oxygen-enhanced MR ventilation imaging of the lung: preliminary clinical experience in 25 subjects. AJR Am J Roentgenol 2001;177: 185–194.

82. Loffler R, Muller CJ, Peller M, et al. Optimization and evaluation of the signal intensity change in multisection oxygen-enhanced MR lung imaging. Magn Reson Med 2000;43:860–866.

83. Muller CJ, Schwaiblmair M, Scheidler J, et al. Pulmonary diffusing capacity: assessment with oxygen-enhanced lung MR imaging preliminary findings. Radiology 2002;222:499–506.

84. Mai VM, Tutton S, Prasad PV, et al. Computing oxygen-enhanced ventilation maps using correlation analysis. Magn Reson Med 2003; 49:591–594.

85. Dietrich O, Losert C, Attenberger U, et al. Fast oxygen-enhanced multislice imaging of the lung using parallel acquisition techniques. Magn Reson Med 2005;53:1317–1325.

86. Chen Q, Jakob PM, Griswold MA, Levin DL, Hatabu H, Edelman RR. Oxygen enhanced MR ventilation imaging of the lung. Magma 1998; 7:153–161.

87. Couch MJ, Ball IK, Li T, et al. Pulmonary ultrashort echo time 19F MR imaging with inhaled fluorinated gas mixtures in healthy volunteers: feasibility. Radiology 2013;269:903–909.

88. Kuethe DO, Caprihan A, Gach HM, Lowe IJ, Fukushima E. Imaging obstructed ventilation with NMR using inert fluorinated gases. J Appl Physiol 2000;88:2279–2286.

89. Cho A. Physics. Helium-3 shortage could put freeze on low-temperature research. Science 2009;326:778–779.

90. Woods JC. Mine the moon for 3He MRI? Not yet. J Appl Physiol 2013;114:705–706.

91. Ruset IC, Ketel S, Hersman FW. Optical pumping system design for large production of hyperpolarized. Phys Rev Lett 2006;96:053002.

92. Hersman FW, Ruset IC, Ketel S, et al. Large production system for hyperpolarized 129Xe for human lung imaging studies. Acad Radiol 2008;15:683–692.

93. Kirby M, Parraga G. Pulmonary functional imaging using hyperpolarized noble gas MRI: six years of start-up experience at a single site. Acad Radiol 2013;20:1344–1356.

94. Emami K, Kadlecek SJ, Woodburn JM, et al. Improved technique for measurement of regional fractional ventilation by hyperpolarized 3He MRI. Magn Reson Med 2010;63:137–150.

95. Horn FC, Tahir BA, Stewart NJ, et al. Lung ventilation volumetry with same-breath acquisition of hyperpolarized gas and proton MRI. NMR Biomed 2014;27:1461–1467.

96. Altes TA, Gersbach JC, Mata JF, III JPM, Brookeman JR, Lange EEd. Evaluation of the safety of hyperpolarized helium-3 gas as an inhaled contrast agent for MRI. In: Proc 15 Annual Meeting ISMRM, Seattle; 2007. p 1305.

97. Lutey BA, Lefrak SS, Woods JC, et al. Hyperpolarized 3He MR imaging: physiologic monitoring observations and safety considerations in 100 consecutive subjects. Radiology 2008;248:655–661.

98. Driehuys B, Martinez-Jimenez S, Cleveland ZI, et al. Chronic obstructive pulmonary disease: safety and tolerability of hyperpolarized 129Xe MR imaging in healthy volunteers and patients. Radiology 2012;262:279–289.

99. Altes TA, Mata J, de Lange EE, Brookeman JR, Mugler JP 3rd. Assessment of lung development using hyperpolarized helium-3 diffusion MR imaging. J Magn Reson Imaging JMRI 2006;24:1277–1283.

100. Liszewski MC, Hersman FW, Altes TA, et al. Magnetic resonance imaging of pediatric lung parenchyma, airways, vasculature, ventilation, and perfusion: state of the art. Radiol Clin N Am 2013;51:555–582.

101. Cadman RV, Lemanske RF Jr, Evans MD, et al. Pulmonary 3He magnetic resonance imaging of childhood asthma. J Allergy Clin Immunol 2013;131:369–376 e361–365.

102. Nikolaou P, Coffey AM, Walkup LL, et al. Near-unity nuclear polarization with an open-source 129Xe hyperpolarizer for NMR and MRI. Proc Natl Acad Sci U S A 2013;110:14150–14155.

103. Nikolaou P, Coffey AM, Walkup LL, et al. A 3D-printed high power nuclear spin polarizer. J Am Chem Soc 2014;136:1636–1642.

104. Halaweish AF, Charles HC. Physiorack: an integrated MRI safe/conditional, gas delivery, respiratory gating, and subject monitoring solution for structural and functional assessments of pulmonary function. J Magn Reson Imaging JMRI 2014;39:735–741.

105. Naish JH, Parker GJ, Beatty PC, et al. Improved quantitative dynamic regional oxygen-enhanced pulmonary imaging using image registration. Magn Reson Med 2005;54:464–469.

106. Dietrich O, Attenberger UI, Ingrisch M, et al. Analysis of signal dynamics in oxygen-enhanced magnetic resonance imaging. Invest Radiol 2010;45:165–173.

107. Ohno Y, Koyama H, Nogami M, et al. Dynamic oxygen-enhanced MRI versus quantitative CT: pulmonary functional loss assessment and clinical stage classification of smoking-related COPD. AJR Am J Roentgenol 2008;190:W93–99.

108. Vaninbroukx J, Bosmans H, Sunaert S, et al. The use of ECG and respiratory triggering to improve the sensitivity of oxygen-enhanced proton MRI of lung ventilation. Eur Radiol 2003;13:1260–1265.

109. Molinari F, Eichinger M, Risse F, et al. Navigator-triggered oxygen-enhanced MRI with simultaneous cardiac and respiratory synchronization for the assessment of interstitial lung disease. J Magn Reson Imaging JMRI 2007;26:1523–1529.

110. Renne J, Lauermann P, Hinrichs J, et al. Clinical use of oxygen-enhanced T1 mapping MRI of the lung: reproducibility and impact of closed versus loose fit oxygen delivery system. J Magn Reson Imaging JMRI 2015;41:60–66.

111. Molinari F, Puderbach M, Eichinger M, et al. Oxygen-enhanced magnetic resonance imaging: influence of different gas delivery methods on the T1-changes of the lungs. Invest Radiol 2008;43:427–432.

112. Dripps RD, Comroe JH. The effect of inhalation of high and of low oxygen concentration upon human respiration and circulation. Am J Med Sci 1947;213:248.

113. Tadamura E, Hatabu H, Li W, Prasad PV, Edelman RR. Effect of oxygen inhalation on relaxation times in various tissues. J Magn Reson Imaging JMRI 1997;7:220–225.

114. Chen Q, Levin DL, Kim D, et al. Pulmonary disorders: ventilation-perfusion MR imaging with animal models. Radiology 1999;213:871–879.

115. Sa RC, Cronin MV, Henderson AC, et al. Vertical distribution of specific ventilation in normal supine humans measured by oxygen-enhanced proton MRI. J Appl Physiol 2010;109:1950–1959.

116. Avants BB, Tustison NJ, Song G, Cook PA, Klein A, Gee JC. A reproducible evaluation of ANTs similarity metric performance in brain image registration. Neuroimage 2011;54:2033–2044.

117. Cook TS, Tustison N, Biederer J, Tetzlaff R, Gee J. How do registration parameters affect quantitation of lung kinematics? In: MICCAI International Conference on Medical Image Computing and Computer-Assisted Intervention 2007;10(Pt 1):817–824.

118. Colegrove FD, Schearer LD, Walters GK. Polarisation of 3He gas by optical pumping. Phys Rev 1963;132:2561–2572.

119. Albert MS, Cates GD, Driehuys B, et al. Biological magnetic resonance imaging using laser-polarized 129Xe. Nature 1994;370:199–201.

120. Middleton H, Black RD, Saam B, et al. MR imaging with hyperpolarized 3He gas. Magn Reson Med 1995;33:271–275.

121. MacFall JR, Charles HC, Black RD, et al. Human lung air spaces: potential for MR imaging with hyperpolarized He-3. Radiology 1996;200:553–558.

122. Kauczor HU, Ebert M, Kreitner KF, et al. Imaging of the lungs using 3He MRI: preliminary clinical experience in 18 patients with and without lung disease. J Magn Reson Imaging JMRI 1997;7:538–543.

123. Möller HE, Chen XJ, Saam B, et al. MRI of the lungs using hyperpolarized noble gases. Magn Reson Med 2002;47:1029–1051.

124. van Beek EJ, Wild JM, Kauczor HU, Schreiber W, Mugler JP 3rd, de Lange EE. Functional MRI of the lung using hyperpolarized 3-helium gas. J Magn Reson Imaging JMRI 2004;20:540–554.

125. Fain SB, Korosec FR, Holmes JH, O'Halloran R, Sorkness RL, Grist TM. Functional lung imaging using hyperpolarized gas MRI. J Magn Reson Imaging JMRI 2007;25:910–923.

126. Emami K, Stephen M, Kadlecek S, Cadman RV, Ishii M, Rizi RR. Quantitative assessment of lung using hyperpolarized magnetic resonance imaging. Proc Am Thorac Soc 2009;6:431–438.

127. Fain SB, Gonzalez-Fernandez G, Peterson ET, et al. Evaluation of structure-function relationships in asthma using multidetector CT and hyperpolarized He-3 MRI. Acad Radiol 2008;15:753–762.

128. Sheikh K, Paulin GA, Svenningsen S, et al. Pulmonary ventilation defects in older never-smokers. J Appl Physiol 2014;117:297–306.

129. Woodhouse N, Wild JM, Paley MN, et al. Combined helium-3/proton magnetic resonance imaging measurement of ventilated lung

volumes in smokers compared to never-smokers. J Magn Reson Imaging JMRI 2005;21:365–369.

130. Mathew L, Evans A, Ouriadov A, et al. Hyperpolarized 3He magnetic resonance imaging of chronic obstructive pulmonary disease: reproducibility at 3.0 Tesla. Acad Radiol 2008;15:1298–1311.

131. van Beek EJ, Dahmen AM, Stavngaard T, et al. Hyperpolarised 3He MRI versus HRCT in COPD and normal volunteers: PHIL trial. Eur Respir J 2009;34:1311–1321.

132. Tzeng YS, Lutchen K, Albert M. The difference in ventilation heterogeneity between asthmatic and healthy subjects quantified using hyperpolarized 3He MRI. J Appl Physiol 2009;106:813–822.

133. Virgincar RS, Cleveland ZI, Kaushik SS, et al. Quantitative analysis of hyperpolarized 129Xe ventilation imaging in healthy volunteers and subjects with chronic obstructive pulmonary disease. NMR Biomed 2013;26:424–435.

134. Fain SB, Panth SR, Evans MD, et al. Early emphysematous changes in asymptomatic smokers: detection with 3He MR imaging. Radiology 2006;239:875–883.

135. Quirk JD, Lutey BA, Gierada DS, et al. In vivo detection of acinar microstructural changes in early emphysema with (3)He lung morphometry. Radiology 2011;260:866–874.

136. Kirby M, Owrangi A, Svenningsen S, et al. On the role of abnormal DL(CO) in ex-smokers without airflow limitation: symptoms, exercise capacity and hyperpolarised helium-3 MRI. Thorax 2013;68:752–759.

137. Tustison NJ, Avants BB, Flors L, et al. Ventilation-based segmentation of the lungs using hyperpolarized (3)He MRI. J Magn Reson Imaging JMRI 2011;34:831–841.

138. Kirby M, Heydarian M, Svenningsen S, et al. Hyperpolarized 3He magnetic resonance functional imaging semiautomated segmentation. Acad Radiol 2012;19:141–152.

139. Niles DJ, Kruger SJ, Dardzinski BJ, et al. Exercise-induced bronchoconstriction: reproducibility of hyperpolarized 3He MR imaging. Radiology 2013;266:618–625.

140. He M, Kaushik SS, Robertson SH, et al. Extending semiautomatic ventilation defect analysis for hyperpolarized (129)xe ventilation MRI. Acad Radiol 2014;21:1530–1541.

141. de Lange EE, Altes TA, Patrie JT, et al. Changes in regional airflow obstruction over time in the lungs of patients with asthma: evaluation with 3He MR imaging. Radiology 2009;250:567–575.

142. Kirby M, Svenningsen S, Ahmed H, et al. Quantitative evaluation of hyperpolarized helium-3 magnetic resonance imaging of lung function variability in cystic fibrosis. Acad Radiol 2011;18:1006–1013.

143. de Lange EE, Altes TA, Patrie JT, et al. Evaluation of asthma with hyperpolarized helium-3 MRI: correlation with clinical severity and spirometry. Chest 2006;130:1055–1062.

144. Kruger SJ, Niles DJ, Dardzinski BJ. Hyperpolarized helium-3 MRI exercise-induced bronchoconstriction during challenge and therapy. J Magn Reson Med 2014;39:1230–1237.

145. Kirby M, Pike D, Coxson HO, McCormack DG, Parraga G. Hyperpolarized (3)he ventilation defects used to predict pulmonary exacerbations in mild to moderate chronic obstructive pulmonary disease. Radiology 2014;273:887–896.

146. Svenningsen S, Kirby M, Starr D, et al. Hyperpolarized (3) He and (129) Xe MRI: differences in asthma before bronchodilation. J Magn Reson Imaging JMRI 2013;38:1521–1530.

147. Kirby M, Svenningsen S, Kanhere N, et al. Pulmonary ventilation visualized using hyperpolarized helium-3 and xenon-129 magnetic resonance imaging: differences in COPD and relationship to emphysema. J Appl Physiol 2013;114:707–715.

148. Diaz S, Casselbrant I, Piitulainen E, et al. Hyperpolarized 3He apparent diffusion coefficient MRI of the lung: reproducibility and volume dependency in healthy volunteers and patients with emphysema. J Magn Reson Imaging JMRI 2008;27:763–770.

149. Halaweish AF, Hoffman EA, Thedens DR, Fuld MK, Sieren JP, van Beek EJ. Effect of lung inflation level on hyperpolarized 3He apparent diffusion coefficient measurements in never-smokers. Radiology 2013;268:572–580.

150. Diaz S, Casselbrant I, Piitulainen E, et al. Progression of emphysema in a 12-month hyperpolarized 3He-MRI study: lacunarity analysis provided a more sensitive measure than standard ADC analysis. Acad Radiol 2009;16:700–707.

151. Kaushik SS, Cleveland ZI, Cofer GP, et al. Diffusion-weighted hyperpolarized 129Xe MRI in healthy volunteers and subjects with chronic obstructive pulmonary disease. Magn Reson Med 2011;65:1154–1165.

152. Fain SB, Altes TA, Panth SR, et al. Detection of age-dependent changes in healthy adult lungs with diffusion-weighted 3He MRI. Acad Radiol 2005;12:1385–1393.

153. Salerno M, de Lange EE, Altes TA, Truwit JD, Brookeman JR, Mugler JP 3rd. Emphysema: hyperpolarized helium 3 diffusion MR imaging of the lungs compared with spirometric indexes—initial experience. Radiology 2002;222:252–260.

154. Chen XJ, Moller HE, Chawla MS, et al. Spatially resolved measurements of hyperpolarized gas properties in the lung in vivo. Part I: diffusion coefficient. Magn Reson Med 1999;42:721–728.

155. Narayanan M, Beardsmore CS, Owers-Bradley J, et al. Catch-up alveolarization in ex-preterm children: evidence from (3)He magnetic resonance. Am J Respir Crit Care Med 2013;187:1104–1109.

156. Hajari AJ, Yablonskiy DA, Sukstanskii AL, Quirk JD, Conradi MS, Woods JC. Morphometric changes in the human pulmonary acinus during inflation. J Appl Physiol 2012;112:937–943.

157. Woods JC, Choong CK, Yablonskiy DA, et al. Hyperpolarized 3He diffusion MRI and histology in pulmonary emphysema. Magn Reson Med 2006;56:1293–1300.

158. Parra-Robles J, Ajraoui S, Deppe MH, Parnell SR, Wild JM. Experimental investigation and numerical simulation of 3He gas diffusion in simple geometries: implications for analytical models of 3He MR lung morphometry. J Magn Reson 2010;204:228–238.

159. Parra-Robles J, Ajraoui S, Marshall H, Deppe MH, Xu X, Wild JM. The influence of field strength on the apparent diffusion coefficient of 3He gas in human lungs. Magn Reson Med 2012;67:322–325.

160. Parra-Robles J, Wild JM. The influence of lung airways branching structure and diffusion time on measurements and models of short-range 3He gas MR diffusion. J Magn Reson 2012;225:102–113.

161. Yablonskiy DA, Sukstanskii AL, Conradi MS. Commentary on The influence of lung airways branching structure and diffusion time on measurements and models of short-range 3He gas MR diffusion. J Magn Reson 2014;239:139–142.

162. Parra-Robles J, Wild JM. Response to Commentary on The influence of lung airways branching structure and diffusion time on measurements and models of short-range 3He gas MR diffusion. J Magn Reson 2014;239:143–146.

163. Narayanan M, Owers-Bradley J, Beardsmore CS, Kuehni CE, Silverman M. Reply: On the use of 3He diffusion magnetic resonance as evidence of neo-alveolarization during childhood and adolescence. Am J Respir Crit Care Med 2014;189:502–504.

164. Parra-Robles J, Wild JM. On the use of 3He diffusion magnetic resonance as evidence of neo-alveolarization during childhood and adolescence. Am J Respir Crit Care Med 2014;189:501–502.

165. Deninger AJ, Eberle B, Ebert M, et al. Quantification of regional intrapulmonary oxygen partial pressure evolution during apnea by (3)He MRI. J Magn Reson 1999;141:207–216.

166. Deninger AJ, Eberle B, Bermuth J, et al. Assessment of a single-acquisition imaging sequence for oxygen-sensitive (3)He-MRI. Magn Reson Med 2002;47:105–114.

167. Rizi RR, Baumgardner JE, Ishii M, et al. Determination of regional VA/Q by hyperpolarized 3He MRI. Magn Reson Med 2004;52:65–72.

168. Miller GW, Mugler JP 3rd, Altes TA, et al. A short-breath-hold technique for lung pO2 mapping with 3He MRI. Magn Reson Med 2010; 63:127–136.

169. Marshall H, Parra-Robles J, Deppe MH, Lipson DA, Lawson R, Wild JM. He pO mapping is limited by delayed-ventilation and diffusion in chronic obstructive pulmonary disease. Magn Reson Med 2014; 71:1172–1178.

170. Hamedani H, Kadlecek SJ, Ishii M, et al. A variability study of regional alveolar oxygen tension measurement in humans using hyperpolarized (3) He MRI. Magn Reson Med 2013;70:1557–1566.

171. Hamedani H, Kadlecek SJ, Ishii M, et al. Alterations of regional alveolar oxygen tension in asymptomatic current smokers: assessment with hyperpolarized He MR imaging. Radiology 2014:132809.

172. Wolber J, Cherubini A, Leach MO, Bifone A. Hyperpolarized 129Xe NMR as a probe for blood oxygenation. Magn Reson Med 2000;43:491–496.

173. Chang YV. MOXE: a model of gas exchange for hyperpolarized 129Xe magnetic resonance of the lung. Magn Reson Med 2013;69: 884–890.

174. Driehuys B, Cofer GP, Pollaro J, Mackel JB, Hedlund LW, Johnson GA. Imaging alveolar-capillary gas transfer using hyperpolarized 129Xe MRI. Proc Natl Acad Sci U S A 2006;103:18278–18283.

175. Kaushik SS, Freeman MS, Yoon SW, et al. Measuring diffusion limitation with a perfusion-limited gas—hyperpolarized 129Xe gas-transfer spectroscopy in patients with idiopathic pulmonary fibrosis. J Appl Physiol 2014;117:577–585.

176. Cleveland ZI, Cofer GP, Metz G, et al. Hyperpolarized Xe MR imaging of alveolar gas uptake in humans. PLoS One 2010;5:e12192.

177. Patz S, Muradian I, Hrovat MI, et al. Human pulmonary imaging and spectroscopy with hyperpolarized 129Xe at 0.2T. Acad Radiol 2008; 15:713–727.

178. Chang YV, Quirk JD, Ruset IC, Atkinson JJ, Hersman FW, Woods JC. Quantification of human lung structure and physiology using hyperpolarized 129Xe. Magn Reson Med 2014;71:339–344.

179. Altes TA, Powers PL, Knight-Scott J, et al. Hyperpolarized 3He MR lung ventilation imaging in asthmatics: preliminary findings. J Magn Reson Imaging JMRI 2001;13:378–384.

180. Samee S, Altes T, Powers P, et al. Imaging the lungs in asthmatic patients by using hyperpolarized helium-3 magnetic resonance: assessment of response to methacholine and exercise challenge. J Allergy Clin Immunol 2003;111:1205–1211.

181. Kirby M, Mathew L, Wheatley A, Santyr GE, McCormack DG, Parraga G. Chronic obstructive pulmonary disease: longitudinal hyperpolarized (3)He MR imaging. Radiology 2010;256:280–289.

182. Mentore K, Froh DK, de Lange EE, Brookeman JR, Paget-Brown AO, Altes TA. Hyperpolarized HHe 3 MRI of the lung in cystic fibrosis: assessment at baseline and after bronchodilator and airway clearance treatment. Acad Radiol 2005;12:1423–1429.

183. Paulin GA, Svenningsen S, Jobse BN, et al. Differences in hyperpolarized He ventilation imaging after 4 years in adults with cystic fibrosis. J Magn Reson Imaging JMRI 2015;41:1701–1707.

184. Morbach AE, Gast KK, Schmiedeskamp J, et al. Diffusion-weighted MRI of the lung with hyperpolarized helium-3: a study of reproducibility. J Magn Reson Imaging JMRI 2005;21:765–774.

185. Diaz S, Casselbrant I, Piitulainen E, et al. Validity of apparent diffusion coefficient hyperpolarized 3He-MRI using MSCT and pulmonary function tests as references. Eur J Radiol 2009;71:257–263.

186. Wang C, Mugler JP 3rd, de Lange EE, Patrie JT, Mata JF, Altes TA. Lung injury induced by secondhand smoke exposure detected with hyperpolarized helium-3 diffusion MR. J Magn Reson Imaging JMRI 2014;39:77–84.

187. Kirby M, Kanhere N, Etemad-Rezai R, McCormack DG, Parraga G. Hyperpolarized helium-3 magnetic resonance imaging of chronic obstructive pulmonary disease exacerbation. J Magn Reson Imaging JMRI 2013;37:1223–1227.

188. de Lange EE, Altes TA, Patrie JT, et al. The variability of regional airflow obstruction within the lungs of patients with asthma: assessment with hyperpolarized helium-3 magnetic resonance imaging. J Allergy Clin Immunol 2007;119:1072–1078.

189. Castro M, Fain SB, Hoffman EA, et al. Lung imaging in asthmatic patients: the picture is clearer. J Allergy Clin Immunol 2011;128: 467–478.

190. Castro M, Woods J. Insights into pediatric asthma with hyperpolarized magnetic resonance imaging of the lung. J Allergy Clin Immunol 2013;131:377–378.

191. Teague WG, Tustison NJ, Altes TA. Ventilation heterogeneity in asthma. J Asthma 2014;51:677–684.

192. Wang C, Altes TA, Mugler JP 3rd, et al. Assessment of the lung microstructure in patients with asthma using hyperpolarized 3He diffusion MRI at two time scales: comparison with healthy subjects and patients with COPD. J Magn Reson Imaging JMRI 2008;28:80–88.

193. Johansson MW, Kruger SJ, Schiebler ML, et al. Markers of vascular perturbation correlate with airway structural change in asthma. Am J Respir Crit Care Med 2013;188:167–178.

194. Marozkina NV, Wang XQ, Stsiapura V, et al. Phenotype of asthmatics with increased airway S-nitrosoglutathione reductase activity. Eur Respir J 2015;45:87–97.

195. Snell GI, Holsworth L, Borrill ZL, et al. The potential for bronchoscopic lung volume reduction using bronchial prostheses: a pilot study. Chest 2003;124:1073–1080.

196. Mathew L, Kirby M, Farquhar D, et al. Hyperpolarized 3He functional magnetic resonance imaging of bronchoscopic airway bypass in chronic obstructive pulmonary disease. Can Respir J 2012;19:41–43.

197. Cox G, Thomson NC, Rubin AS, et al. Asthma control during the year after bronchial thermoplasty. N Engl J Med 2007;356:1327–1337.

198. Ireland RH, Bragg CM, McJury M, et al. Feasibility of image registration and intensity-modulated radiotherapy planning with hyperpolarized helium-3 magnetic resonance imaging for non-small-cell lung cancer. Int J Radiat Oncol Biol Phys 2007;68:273–281.

199. Ireland RH, Woodhouse N, Hoggard N, et al. An image acquisition and registration strategy for the fusion of hyperpolarized helium-3 MRI and x-ray CT images of the lung. Phys Med Biol 2008;53:6055–6063.

200. Bates EL, Bragg CM, Wild JM, Hatton MQ, Ireland RH. Functional image-based radiotherapy planning for non-small cell lung cancer: A simulation study. Radiother Oncol 2009;93:32–36.

201. Hodge CW, Tome WA, Fain SB, Bentzen SM, Mehta MP. On the use of hyperpolarized helium MRI for conformal avoidance lung radiotherapy. Med Dosim 2010;35:297–303.

202. Tahir BA, Swift AJ, Marshall H, et al. A method for quantitative analysis of regional lung ventilation using deformable image registration of CT and hybrid hyperpolarized gas/(1)H MRI. Phys Med Biol 2014; 59:7267–7277.

203. Cai J, McLawhorn R, Altes TA, et al. Helical tomotherapy planning for lung cancer based on ventilation magnetic resonance imaging. Med Dosim 2011;36:389–396.

204. Rinck PA, Petersen SB, Lauterbur PC. NMR imaging of fluorine-containing substances. RoFo 1984;140:239–243.

205. Noth U, Morrissey SP, Deichmann R, et al. In vivo measurement of partial oxygen pressure in large vessels and in the reticuloendothelial system using fast 19F-MRI. Magn Reson Med 1995;34:738–745.

206. Pratt RG, Zheng J, Stewart BK, et al. Application of a 3D volume 19F MR imaging protocol for mapping oxygen tension (pO2) in perfluorocarbons at low field. Magn Reson Med 1997;37:307–313.

207. Amis TC, Jones HA, Hughes JM. Effect of posture on inter-regional distribution of pulmonary ventilation in man. Respir Physiol 1984;56: 145–167.

208. Wagner PD, Saltzman HA, West JB. Measurement of continuous distributions of ventilation-perfusion ratios: theory. J Appl Physiol 1974; 36:588–599.

209. Ouriadov AV, Fox MS, Couch MJ, Li T, Ball IK, Albert MS. In vivo regional ventilation mapping using fluorinated gas MRI with an x-centric FGRE method. Magn Reson Med 2015 [Epub ahead of print].

210. Kruger SJ. 3D radial oxygen enhanced imaging in normal and asthmatic human subjects. In: Proc 21st Annual Meeting ISMRM, Salt Lake City; 2013.

211. Petersson J, Rohdin M, Sanchez-Crespo A, et al. Posture primarily affects lung tissue distribution with minor effect on blood flow and ventilation. Respir Physiol Neurobiol 2007;156:293–303.

212. Yablonskiy DA, Sukstanskii AL, Leawoods JC, et al. Quantitative in vivo assessment of lung microstructure at the alveolar level with hyperpolarized 3He diffusion MRI. Proc Natl Acad Sci U S A 2002; 99:3111–3116.

213. Chen XJ, Hedlund LW, Moller HE, Chawla MS, Maronpot RR, Johnson GA. Detection of emphysema in rat lungs by using magnetic resonance measurements of 3He diffusion. Proc Natl Acad Sci U S A 2000;97:11478–11481.

214. Couch MJ, Ball IK, Li T, et al. Inert fluorinated gas MRI: a new pulmonary imaging modality. NMR Biomed 2014;27:1525–1534.

215. Adolphi NL, Kuethe DO. Quantitative mapping of ventilation-perfusion ratios in lungs by 19F MR imaging of T1 of inert fluorinated gases. Magn Reson Med 2008;59:739–746.

216. Jacob RE, Chang YV, Choong CK, et al. 19F MR imaging of ventilation and diffusion in excised lungs. Magn Reson Med 2005;54:577–585.

217. Ohno Y, Hatabu H, Takenaka D, Van Cauteren M, Fujii M, Sugimura K. Dynamic oxygen-enhanced MRI reflects diffusing capacity of the lung. Magn Reson Med 2002;47:1139–1144.

218. Tedjasaputra V, Sa RC, Arai TJ, et al. The heterogeneity of regional specific ventilation is unchanged following heavy exercise in athletes. J Appl Physiol 2013;115:126–135.

219. Lewis SM, Evans JW, Jalowayski AA. Continuous distributions of specific ventilation recovered from inert gas washout. J Appl Physiol 1978;44:416–423.

220. Kaneko K, Milic-Emili J, Dolovich MB, Dawson A, Bates DV. Regional distribution of ventilation and perfusion as a function of body position. J Appl Physiol 1966;21:767–777.

221. Nakagawa T, Sakuma H, Murashima S, Ishida N, Matsumura K, Takeda K. Pulmonary ventilation-perfusion MR imaging in clinical patients. J Magn Reson Imaging JMRI 2001;14:419–424.

222. Ohno Y, Hatabu H, Higashino T, et al. Oxygen-enhanced MR imaging: correlation with postsurgical lung function in patients with lung cancer. Radiology 2005;236:704–711.

223. Kruger SJ. Comparison of regional ventilation defect distribution between oxygen-enhanced and hyperpolarized He-3 MRI. In: Proc 22nd Annual Meeting ISMRM, Milan; 2014.

224. Ohno Y, Hatabu H. Basics concepts and clinical applications of oxygen-enhanced MR imaging. Eur J Radiol 2007;64:320–328.

225. Ohno Y, Iwasawa T, Seo JB, et al. Oxygen-enhanced magnetic resonance imaging versus computed tomography: multicenter study for clinical stage classification of smoking-related chronic obstructive pulmonary disease. Am J Respir Crit Care Med 2008;177:1095–1102.

226. Ohno Y, Nishio M, Koyama H, et al. Oxygen-enhanced MRI, thin-section MDCT, and perfusion SPECT/CT: comparison of clinical implications to patient care for lung volume reduction surgery. AJR Am J Roentgenol 2012;199:794–802.

227. Ohno Y, Koyama H, Matsumoto K, et al. Oxygen-enhanced MRI vs. quantitatively assessed thin-section CT: pulmonary functional loss assessment and clinical stage classification of asthmatics. Eur J Radiol 2011;77:85–91.

228. Ohno Y, Nishio M, Koyama H, et al. Asthma: comparison of dynamic oxygen-enhanced MR imaging and quantitative thin-section CT for evaluation of clinical treatment. Radiology 2014:132660.

229. Renne J, Hinrichs J, Schonfeld C, et al. Noninvasive quantification of airway inflammation following segmental allergen challenge with functional MR imaging: a proof of concept study. Radiology 2015; 274:267–275.

230. Yu H, Zhao S, Hoffman EA, Wang G. Ultra-low dose lung CT perfusion regularized by a previous scan. Acad Radiol 2009;16:363–373.

231. Goo HW. Dual-energy lung perfusion and ventilation CT in children. Pediatr Radiol 2013;43:298–307.

232. Kim WW, Lee CH, Goo JM, et al. Xenon-enhanced dual-energy CT of patients with asthma: dynamic ventilation changes after methacholine and salbutamol inhalation. AJR Am J Roentgenol 2012;199: 975–981.

233. Wielputz MO, Puderbach M, Kopp-Schneider A, et al. Magnetic resonance imaging detects changes in structure and perfusion, and response to therapy in early cystic fibrosis lung disease. Am J Respir Crit Care Med 2014;189:956–965.

234. Cussler EL. Diffusion: Mass transfer in fluid systems. Diffusion: mass transfer in fluid systems. Cambridge, UK: Cambridge University Press; 2009.

235. Weathersby PK, Homer LD. Solubility of inert gases in biological fluids and tissues: a review. Undersea Biomed Res 1980;7:277–296.

236. Kabalnov. Gas emulsions stabilized with fluorinated ethers having low Ostwald coefficients. Greeley, CO: Alliance Pharmaceutical Group; 1998.

237. Kauczor H, Surkau R, Roberts T. MRI using hyperpolarized noble gases. Eur Radiol 1998;8:820–827.

238. Kober F, Koenigsberg B, Belle V, et al. NMR imaging of thermally polarized helium-3 gas. J Magn Reson 1999;138:308–312.

239. Zhao L, Mulkern R, Venkatesh A, Gudbjartsson H, Jolesz F, Albert M. Hyperpolarized Xe-129 T2 and diffusion measurements for fast spin-echo MRI. In: Proc 6th Annual Meeting ISMRM, Sydney; 1998.

240. Morris AH, Blatter DD, Case TA, et al. A new nuclear magnetic resonance property of lung. J Appl Physiol 1985;58:759–762.

241. Saam B, Yablonskiy DA, Gierada DS, Conradi MS. Rapid imaging of hyperpolarized gas using EPI. Magn Reson Med 1999;42:507–514.